Robotica (2024), **42**, pp. 3102–3131
doi:10.1017/S0263574724001309

CAMBRIDGE UNIVERSITY PRESS

RESEARCH ARTICLE

Motion control of legged robots based on gradient central pattern generators

Yihui Zhang[1], Wenshuo Liu[2] and Ning Tan[2]

[1]School of Computer Science and Engineering, Sun Yat-sen University, Guangzhou, China
[2]Key Laboratory of Machine Intelligence and Advanced Computing, Ministry of Education, Sun Yat-sen University, Guangzhou, China
Corresponding author: Ning Tan; Email: tann5@mail.sysu.edu.cn

Received: 25 April 2024; **Revised:** 11 June 2024; **Accepted:** 30 June 2024; **First published online:** 18 October 2024

Keywords: Central pattern generator; legged robot; locomotion control; vestibular sensory feedback; differential evolutionary

Abstract

The design of motion control systems for legged robots has always been a challenge. This article first proposes a motion control method for legged robots based on the gradient central pattern generator (GD-CPG). The periodic signals output from the GD-CPG neural network are used as the drive signals of each thigh joint of the legged robots, which are then converted into the driving signal of the knee and ankle joints by the thigh–knee mapping function and the knee–ankle mapping function. The proposed control algorithm is adapted to quadruped and hexapod robots. To improve the ability of legged robots to cope with complex terrains, this article further proposes the responsive gradient-CPG motion control method for legged robots. From the perspective of bionics, a biological vestibular sensory feedback mechanism is established in the control system. The mechanism adjusts the robot's motion state in real time through the attitude angle of the body measured during the robot's motion, to keep the robot's body stable when it moves in rugged terrains. Compared with the traditional feedback model that only balances the body pitch, this article also adds the balancing functions of body roll and yaw to balance the legged robot's motion from more dimensions and improve the linear motion capability. This article also introduces a differential evolutionary algorithm and designs a fitness function to adaptively optimize vestibular sensory feedback parameters. The validity, robustness, and transferability of the method are verified through simulations and physical experiments.

1. Introduction

Mobile robots use a variety of motion methods in different environments, such as wheeled, tracked, legged, hybrid, and bionic. Of the existing solutions, legged robots are pertained walking across complex terrains due to the discrete footholds and ability to move in any direction [1, 2]. Legged robots are a class of robots that imitate the movement of animals and use legs to complete the move, offering advantages such as strong adaptability to the environment, flexible movement, active vibration isolation, and low energy consumption.

The ability to move flexibly in complex and changing environments is a key capability for animals. Similarly, giving effective mobility to robots doing assignments in various conditions is essential [3]. However, traditional model-based control through numerical, kinematic, and geometric techniques is not always appropriate for dynamic and changing conditions yet requires high dependability and adaptability [4]. Thus, the locomotion control issue is an area in which biology and robotics should collaborate intently [5].

Organisms with fixed forms of motion have widespread periodic movements, such as walking, running, swimming, jumping, flying, and other physical movements, as well as physiological behaviors, such as chewing, breathing, heartbeat, and gastrointestinal peristalsis, which are characterized by periodic movements. Biologists typically assume that the rhythmic motion of animals is a self-produced

© The Author(s), 2024. Published by Cambridge University Press.

https://doi.org/10.1017/S0263574724001309 Published online by Cambridge University Press

behavior of low-level nerve centers regulated by the central pattern generator (CPG) located at the thoracic-ventral ganglion of vertebrates or invertebrates [6–10]. CPG are distributed oscillatory networks made up of intermediate neurons, which generate multiple or single periodic signals with stable phase interlocking relationships by mutual suppression among neurons to regular the rhythmic movements of the limbs or relevant parts of the body. The synaptic connections between the neurons in the CPG are adaptable and can generate different output patterns, allowing the animal to show a variety of rhythmic motor behaviors [11]. Using CPG models as motion controllers for various types of robots has become the preferred choice of many researchers [12–14]. The motion of legged robots has strong rhythmic characteristics. Many CPG models have been proposed previously, such as Van der Pol oscillator model [15], Matsuoka oscillator model [16, 17], Hopf oscillator model [18, 19], Kuramoto oscillator model [20, 21], etc. Bipedal robots are robots in humanoid form. They move with a small contact area with the ground and have poor static stability. Jo et al. [22] proposed a robust walking stabilization strategy of humanoids on uneven terrain via a QP-based impedance/admittance control. The core idea is combining impedance control (IC) and hybrid admittance control (HAC) which are proposed to enhance walking stability. Yat et al. [23] predicted and adjusted the foot-end landing position for external perturbations at each time during the bipedal robot's motion, and then tracked the task trajectory using a QP-based task space whole-body controller while satisfying specific physical constraints. To analyze the walking motion of a bipedal robot, Fazel et al. [24] proposed a new method called "passive gait-based trajectory design (PGBTD)" to determine the desired walking trajectory of the robot for one step. Considering the nonlinearity of the examined system, an optimal control method based on the state-dependent Riccati equation (SDRE) is employed to track the desired trajectory obtained. This improves the control efficiency of bipedal robots in complex environments. The motion control of a quadruped robot can be accomplished by using a CPG oscillator network to output four periodic signals. Zheng et al. [25] used the Matsuoka-CPG model as the motion control core of a quadruped robot to realize walking, trotting, and galloping gaits of a quadruped robot. Most researchers only focus on the control of the leg joints of the quadruped robot, ignoring the influence of the body (spine) on the robot's motion. Zhang et al. [26] proposed a multimodel fusion control method based on the task decomposition idea and the CPG model for a 2-degree-of-freedom active spine-jointed faux cheetah quadruped robot. The method realizes single-leg jumping control with a spring-loaded inverted pendulum model, coordinated control among four legs as well as spine legs through CPG, and realizes complex terrain motion and gait transformation in a simulation environment to verify the validity of the model. Due to the number of legs and low chassis, the stability of hexapod robots is better than that of bipedal and quadruped robots, and they are more suitable for performing tasks in some complex environments. Generally speaking, each leg of a hexapod robot has 3 degrees of freedom and there are 18 degrees of freedom in total. How to realize the coordinated control of these legs is the focus of hexapod robot control. Matsuoka-CPG and VDP-CPG models are also effective models for realizing the control of hexapod robots [15, 27]. Bal [28] proposed a CPG topology with bidirectional diffusion coupling to improve the gait transition efficiency of a hexapod robot. The effectiveness of the method is verified by experiments in several aspects, such as movement frequency, forward speed, and gait transition time. The introduction of sensory feedback further improves the control performance of the hexapod robot. Barron et al. [29] integrated a visual sensor in the VDP-CPG control loop. This mechanism is used to map the visual perception information to the CPG control parameters, adjust the motion speed of the hexapod robot in real time, and achieve reliable gait transitions. Sartoretti et al. [30], on the other hand, model the inertial feedback mechanism of the organisms in the Hopf-CPG model, to adjust the legs and the body in real time during the motion process postures to cope with various complex terrains.

Research on the stability of legged robots during motion has been the focus, especially when they are moving over rough terrain. Ricardo et al. [31] proposed the use of an SNN-based CPG control method for controlling quadruped and hexapod robots, although the method has not been implemented in a real-world environment. Using the mantis shrimp as a bionic model, Chen et al. [32] designed a CPG-based target tracking system, based on which the bionic mantis robot can quickly adjust the tracking speed and direction according to the horizontal deviation and the target distance, but the control

https://doi.org/10.1017/S0263574724001309 Published online by Cambridge University Press

algorithm has limited robustness due to the hardware limitation. Based on supervised learning, Wu et al. [33] proposed an optimized CPG model based on the DT and RF models of the leg workspace of a legged robot, which can efficiently and quickly achieve real-time gait planning in unknown terrain. In addition, to cope with future planetary exploration missions, Chen et al. [34] proposed a Convolutional Neural Networks (CNN)-based terrain evaluation method based on a bionic ant hexapod robot as a way to accomplish adaptive gait switching and introduce comprehensive performance evaluation indexes including speed and stability, which were experimentally verified to significantly improve the overall performance of the robot in complex terrains; however, as a complex environment control model, the performance evaluation index of this method is single. Furthermore, vestibular sensory feedback is also employed to adjust posture during a motion to enhance the stability of robots [35–38].

The CPG-based control methods also have many disadvantages. One of them is that there are too many parameters to be set for achieving a desired locomotor pattern within a broad search space. Comprehending the connections between parameters and output results, like waveforms, phase hysteresis, and frequency is challenging. The Trial-and-error approach is one of the solutions. In this approach, the parameters are acquired by instinctive principles and improved under simulations and physical experiments. Evolutionary computation method [16, 39–43] is also a common solution. In recent years, supervised and unsupervised learning played a large role in CPG parameter searching. Hu et al. [44] suggested a numerical approach to synthesize the parameters of a CPG network to achieve the desired locomotor patterns. This approach transforms the CPG parameters into dynamic systems that are integrated into the CPG network dynamics. The CPG network with the suggested learning rules can encode the frequency, amplitude, and phase relations of teaching signals. Farzaneh et al. [45] suggested a new supervised learning method called Fourier-based automated learning central pattern generators. For learning rhythmic signals, the rhythmic signal is analyzed using Fourier analysis and fitted with a finite Fourier series. The CPG parameters are determined by direct comparison with the Fourier series.

In summary, CPG models have been widely used in the design of legged robot control systems and have provided much inspiration for this work. However, an adaptive motion control algorithm for legged robots with relatively short online execution time, smooth and fluent gait execution and transition, modeled with biofeedback mechanism, and high transferability, which is the motivation of this paper, has not yet emerged. Bing et al. [46, 47] based on the convergence property of gradient systems, designed a lightweight chained with low structural complexity CPG model, which is the gradient-CPG (GD-CPG), and used it for the control of machine snakes. It is proved experimentally that the machine snake controlled by this method does not generate abnormal moments in the body during the movement. Moreover, compared with the traditional control method that uses a sine wave as the drive signal, the GD-CPG-controlled machine snake can realize a smoother gait transition and higher motion stability. Inspired by this work, this article uses GD-CPG for legged robot control and various optimizations based on this. Specifically, the main contributions of this paper are summarized as follows.

- In this article, GD-CPG is used for the first time to design a control system for legged robots. The output of the CPG oscillator network can be used as a drive signal for the thigh joint of the legged robot, and then it is translated by the motion mapping function to generate the corresponding drive signals for the knee and ankle joints. By adjusting the parameters of the CPG oscillator network, the legged robot can finally exhibit various gait motions.
- Responsive gradient-CPG (RG-CPG) is proposed for legged robot control. A biological vestibular sensory feedback mechanism is modeled based on the GD-CPG to keep the quadruped robot stable when it moves in complex environments. This article also adds the balancing functions of body roll and yaw in the mechanism.
- This article further introduces the differential evolutionary algorithm (DE) and designs an adaptive function to adaptively optimize vestibular sensory feedback parameters. In addition, this article compares the control validity of RG-CPG with other common CPG models for legged robots.

https://doi.org/10.1017/S0263574724001309 Published online by Cambridge University Press

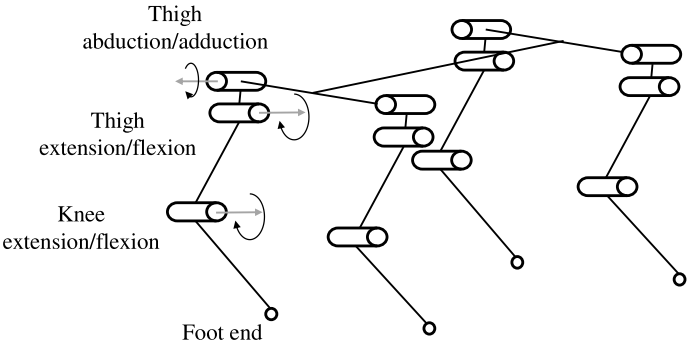


Figure 1. *Full-elbow quadruped robot structure.*

The remainder of this article is organized as follows. In Section 2, the structure of the quadruped robot and hexapod are presented. In Section 3 and Section 4, specific implementation details of GD-CPG and RG-CPG are given. Simulations and physical experiments are illustrated in Section 5 and Section 6. Finally, Section 7 concludes this article.

2. Legged robot structure

2.1. Quadruped robot structure

The mechanical structure has a great influence on the robot's motion performance, and the leg structure is the key to the design of the legged robot mechanism. From the perspective of bionics, it is an effective method to design the mechanical structure of quadruped robots by imitating the body and leg structure characteristics of different quadrupeds. The leg joints of quadrupeds are categorized into two types: knee joint and elbow joint. The knee joint refers to the joint structure in which the apex of the joint faces the forward direction, such as the knee joint of the lower limb of the human body; the elbow joint is the opposite, such as the elbow joint and ankle joint of the human body. The use of these two joint structures to design the leg of a legged robot is a relatively common approach today.

The structure of the full-elbow quadruped robot is shown in Figure 1, which is connected between the body and the legs by the thigh joint with 2 degrees of freedom to realize the deflection and pitch motion of the thighs; and between the thighs and the lower legs by the knee joint with 1 degree of freedom to realize the pitch motion of the lower legs. To simplify the control process, this article investigates the motion control process of thigh and knee extension/flexion (pitching motion) for each leg only. To facilitate the subsequent introduction of gait characteristics, each actuator of the quadruped robot is coded and defined: fore left leg (FL); rear left leg (RL); fore right leg (FR); rear right leg (RR).

2.2. Hexapod robot structure

Hexapod insects have evolved to be able to move in all kinds of complex environments in nature. The design of bionic hexapod robots draws on the body structure of hexapod insects. Compared to bipedal and quadruped robots, hexapods have a more redundant structure and are more stable when traversing unstructured terrain. The mechanical structure of a hexapod robot is similar to that of a quadruped robot and consists of two parts: the body and the leg structure. The most important of these is the way the six legs are distributed in the body and the mechanical structure of the single leg. The hexapod robot structure in this article is a positive hexagonal body layout, with the robot's six legs distributed on six vertices (as shown in Figure 2a). The advantages of this layout include strong steering ability, small interference radius between different legs, and motion diversity; the disadvantage is the short stride distance. The single leg of the hexapod robot uses a common three-joint structure. As shown in

https://doi.org/10.1017/S0263574724001309 Published online by Cambridge University Press

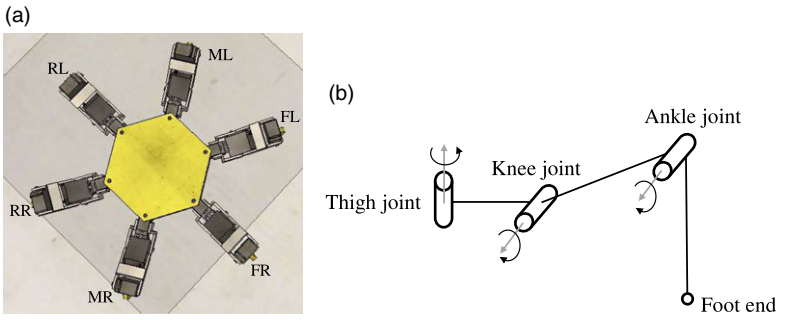


Figure 2. *Structure of the hexapod robot. (a) Layout of the hexapod robot body, (b) single-legged structure of the hexapod robot.*

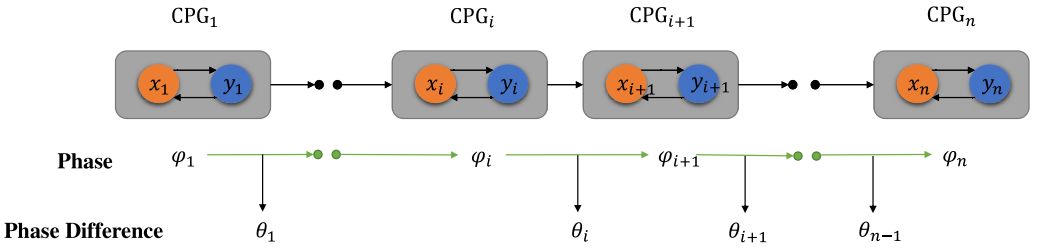


Figure 3. *GD-CPG structure and parameters.*

Figure 2b, the single leg of the hexapod robot consists of three connecting rods and is connected to the foot end by an end rod. The leg is connected to the body and each linkage of the leg by active joints, including the thigh, knee, and ankle joints. The rotation axis of the thigh joint is perpendicular to the body platform to realize the deflection motion of the leg; the rotation axis of the knee and ankle joints is parallel to the body platform to realize the pitching motion of the leg. In this article, each actuator of the hexapod robot is coded and defined: fore left leg (FL); middle left leg (ML); rear left leg (RL); fore right leg (FR); middle right leg (MR); rear right leg (RR).

3. GD-CPG-based motion control method for legged robots

This section focuses on the implementation of the GD-CPG-based motion control method for legged robots.

3.1. CPG model based on gradient method

Chained networks are one of the most common network topologies in CPG models. Bing et al. [46] designed a chain-coupled CPG oscillator model, GD-CPG, whose CPG network convergence behavior is based on a gradient system (the gradient system is derived from the gradient field [48]), which adjusts the frequency, phase difference, and amplitude of the output signal as needed.

As shown in Figure 3, the GD-CPG network consists of n neurons with the same structure and parameters. Assuming that the phase of the ith neuron is φ_i and the phase difference between the neighboring ith and $i+1$th neurons is θ_i, the expected phase difference is $\tilde{\theta}_i$. The single-neuron GD-CPG model can

https://doi.org/10.1017/S0263574724001309 Published online by Cambridge University Press

be written as [46]:

$$\begin{cases} \dot{\varphi}_i = \omega_i + M\{i,:\} \cdot \Phi + N\{i,:\} \cdot \tilde{\Theta} \\ \ddot{r}_i = a_i \left[\frac{a_i}{4}(R_i - r_i) - \dot{r}_i \right] \\ \ddot{c}_i = a_i \left[\frac{a_i}{4}(C_i - c_i) - \dot{c}_i \right] \\ x_i = c_i + r_i \sin(\varphi_i) \end{cases} \tag{1}$$

where,

$$M = \begin{bmatrix} -\mu_1 & \mu_2 & & & 0 \\ \mu_2 & -2\mu_2 & \mu_2 & & \\ & \ddots & \ddots & \ddots & \\ & & \mu_{n-1} & -2\mu_{n-1} & \mu_{n-1} \\ 0 & & & \mu_n & -\mu_n \end{bmatrix}_{n \times n} \tag{2}$$

$$N = \begin{bmatrix} 1 & & 0 \\ -1 & 1 & \\ & -1 & \ddots \\ & & \ddots \quad 1 \\ 0 & & -1 \end{bmatrix}_{n \times (n-1)} \tag{3}$$

In Eq. (1), ω_i is the constant of integration and the frequency of the CPG signal. $M\{i,:\}$ is the ith row vector in Eq. (2), which determines the convergence rate of the CPG signal, where μ_i is the convergence rate coefficient, and the larger the μ_i, the faster the signal converges; $N\{i,:\}$ is the ith rows in Eq. (3). Φ is the phase vector of the CPG neurons, and $\tilde{\Theta}$ is the vector of expected phase differences between the CPG neurons. $\ddot{r}_i$ and $\ddot{c}_i$ are the two PD controllers that guarantee the convergence of the signal amplitude and amplitude deviation, with the positive constants a_i as their convergence coefficients, R_i is the stabilized amplitude of the CPG signal, C_i is the offset value of the stabilized amplitude, and r_i and c_i denote the ith oscillator's signal amplitude and signal amplitude offset, respectively. The state variable φ_i is the phase of the ith oscillator. The variable x_i is the CPG output signal calculated from the phase φ_i, amplitude r_i, and amplitude offset c_i.

3.2. Comparison with other CPG models

Many common CPG models can produce curves with desired characteristics, such as amplitude, frequency, and phase difference. However, the online execution time is rarely examined, which is a critical factor in affecting the CPG models' performance in actual applications. To test the advantages of our adopted GD-CPG model, simulations are performed on MATLAB R2021a to evaluate the online execution time of the CPG models. To ensure accuracy, this article set the number of execution time steps for each CPG model to 400, performed ten simulations for each model separately and calculated the average value. The results are shown in Figure 4. It can be observed that the online execution time of 400-time steps for the gradient CPG model is about 6 ms, much shorter than the online execution times of the other three models. Therefore, the conclusion can be drawn that the gradient CPG model is lightweight in terms of computational load compared with other CPG models.

https://doi.org/10.1017/S0263574724001309 Published online by Cambridge University Press

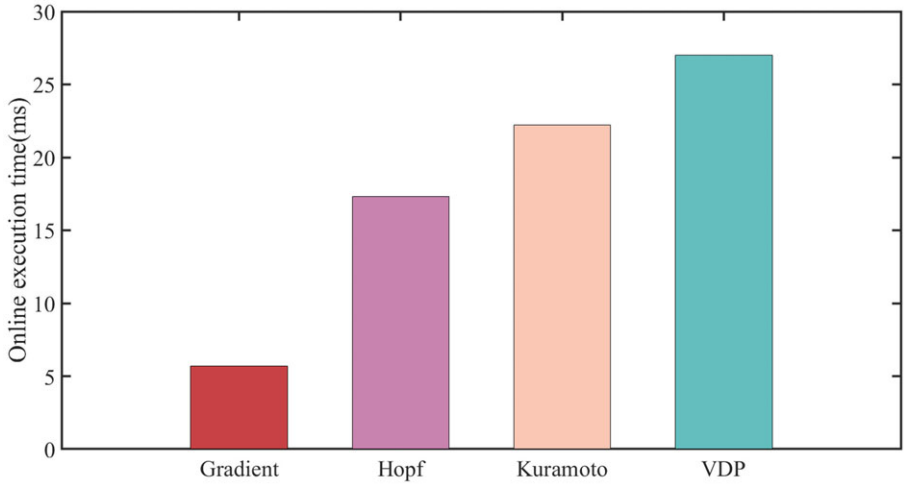


Figure 4. *The execution time on MATLAB R2021a of four kinds of CPG models.*

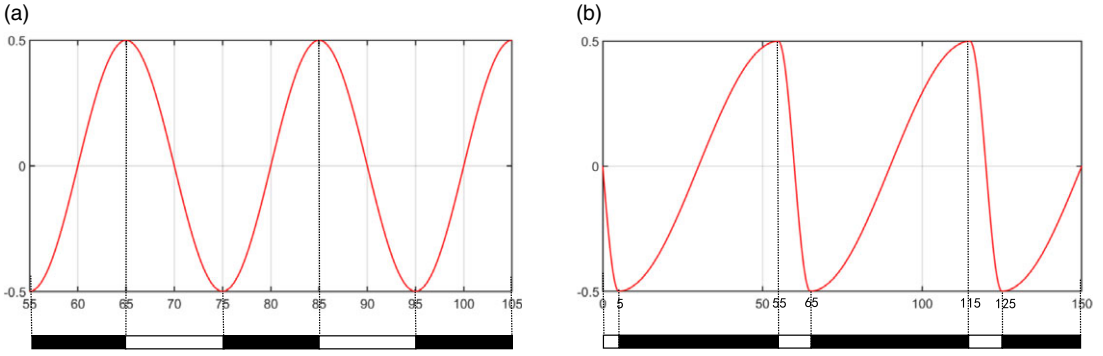


Figure 5. *Legged robot motion gait CPG output waveforms. (a) Walking gait of the quadruped robot, (b) wave gait of the hexapod robot.*

3.3. BI-GD-CPG fitting control model

For the typical gait of the quadruped robot as well as the tripod gait of the hexapod robot, the duty cycle is $\frac{1}{2}$, which means the time occupancy of the support phase and swing phase of either leg is the same in one complete gait cycle, which represents that the driving signals of the thigh joints are symmetric sinusoidal-like waves. As shown in Figure 5a, for the thigh drive signal, the rising phase represents the support phase, the falling phase represents the swing phase, and the CPG output waveform of the quadruped robot's walking gait is a symmetric sinusoidal-like waveform.

However, the tetrapod gait as well as the wave gait duty cycle of the hexapod robot are $\frac{2}{3}$ and $\frac{5}{6}$, respectively. Taking wave gait as an example, the support phase duty cycle of any leg of the hexapod robot is $\frac{5}{6}$ and the swing phase duty cycle is $\frac{1}{6}$ in one complete gait cycle. Therefore, to complete the wave gait, the rising phase should be $\frac{5}{6}$ of the gait cycle time, and the falling phase should be $\frac{1}{6}$ of the gait cycle time (as shown in Figure 5b).

To improve the gait diversity of legged robots, this article proposes a BI-GD-CPG fitting model. The rising and falling phases of the CPG output signal are fitted by two different sinusoidal-like functions. Based on Eq. (1), the BI-GD-CPG output signal is

https://doi.org/10.1017/S0263574724001309 Published online by Cambridge University Press

$$\begin{cases} \dot{\varphi}_i = \omega_i + M\{i,:\} \cdot \Phi + N\{i,:\} \cdot \tilde{\Theta} \\ \ddot{r}_i = a_i \left[\dfrac{a_i}{4}(R_i - r_i) - \dot{r}_i \right] \\ \ddot{c}_i = a_i \left[\dfrac{a_i}{4}(C_i - c_i) - \dot{c}_i \right] \\ x_i = \begin{cases} c_i + r_i \sin(\omega_p x), & \text{swing phase} \\ c_i + r_i \sin(\omega_q x), & \text{support phase} \end{cases} \end{cases} \tag{4}$$

where,

$$\omega_p = \frac{\pi}{10},$$

$$\omega_q = \begin{cases} \dfrac{\pi}{20}, & \text{tetrapod gait} \\ \dfrac{\pi}{50}, & \text{wave gait} \end{cases}.$$

In Eq. (4), x_i is the output of the dual GD-CPG fitting model. The rest of the parameters have the same meaning as in Eq. (1). ω_p and ω_q are the frequencies of the CPG signals of the swing phase and the support phase, respectively. According to the principle of stabilizing and smoothing the control signal, the amplitude and bias of the two sinusoidal functions are the same, and the amplitudes are chosen to be at the great and very small places to be fitted so that the asymmetric CPG output signal can be obtained.

3.4. Motion mapping functions for legged robots

The stability and coordination of legged robot motion largely depend on the joint motion trajectories. Traditional motion control of legged robots is generally realized by planning the foot drop point and inversely calculating the angular displacements of each joint. When using this inverse kinematics method to control a legged robot with redundant degrees of freedom, the computation time is long, resulting in inefficient control. Studying and mimicking the joint motion laws of legged animals from a bionic perspective can simplify the motion design process of legged robots, and the key lies in motion modeling. Specifically, according to the technical characteristics of legged robots, similar animal structures and motion laws are selected as the imitation objects, and the motion model of the animal is derived through observation, calculation, and other methods, based on which mathematical modeling is carried out and finally applied to the control design of legged robots.

3.4.1. Thigh–knee mapping function

For legged animals, under normal locomotion, the thigh and knee joints of the same leg have a fixed phase relationship. During the swing phase, the thigh and knee joints move synchronously. In the front part of the thigh swing, the knee contracted; at the midpoint of the thigh swing, the knee contracted to the greatest extent; in the rear part of the thigh swing, the knee extended; at the end point of the thigh swing, the knee returned to its original position. In the support phase, the knee remains essentially immobile while the thigh rotates backward. Such a thigh and knee joint movement relationship of the legged animal can ensure that the height of the swing leg is always greater than the height of the support leg, and the foot end of the swing leg is always higher than the ground, which will not affect the movement of the body. According to the fixed phase relationship that the thigh and knee joints of the same leg have, the knee joint motion position curve is obtained by flipping and translating the thigh joint motion position curve, and the coupling of the thigh and knee joints is realized. The knee joint motion position function

https://doi.org/10.1017/S0263574724001309 Published online by Cambridge University Press

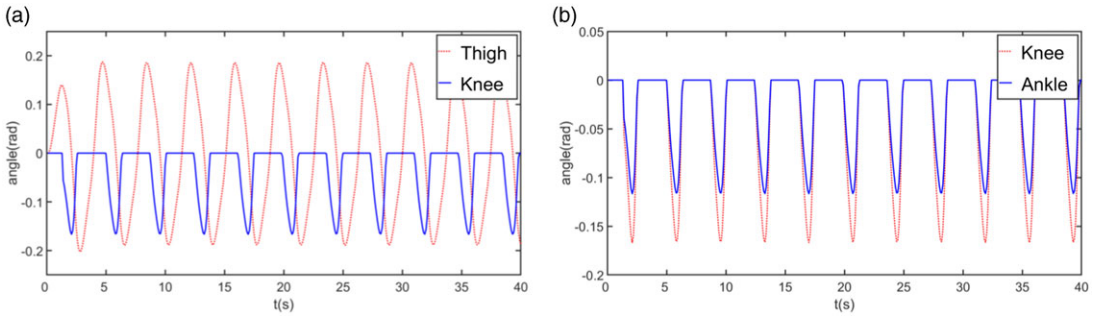


Figure 6. *Legged robot motion mapping function output signals. (a) Thigh–knee mapping function output signal, (b) knee–ankle mapping function output signal.*

is shown in Eq. (5) [25].

$$\begin{cases} \theta_k(t) = \begin{cases} k(t)(A_h - |\theta_h(t)|), & (\dot{\theta}_h \le 0, \text{swing phase}) \\ 0, & (\dot{\theta}_h > 0, \text{support phase}) \end{cases} \\ k(t) = k_0(1 + \dfrac{|\theta_h(t)|}{A_h}) \\ k_0 = \dfrac{A_k}{A_h} \end{cases} \tag{5}$$

where $\theta_h(t)$ and $\theta_k(t)$ are the control signals of the thigh and knee joints at moment t, respectively, $k(t)$ is the variable gain, A_h and A_k are the absolute values of the thigh and knee amplitudes, respectively, and k_0 is the ratio of the absolute knee to thigh amplitudes.

Figure 6a shows the CPG-generated thigh position curve and the knee position curve after thigh–knee mapping. From the figure, it can be seen that the knee joint has motion in the swing phase and no motion in the support phase, and the position curve is like a half-wave, so the thigh-knee mapping function is called a half-wave function.

3.4.2. Knee–ankle mapping function

The hexapod robot has three degrees of freedom in each leg, so ankle joint control is also needed. In this article, the thigh and knee joint motion laws of the hexapod robot are the same as those of the quadruped robot, while the motion law of the ankle joint is closer to that of the knee joint, so the motion position curve of the ankle joint can be obtained by mapping the motion position curve of the knee joint. The knee–ankle mapping function of the legged robot is as follows [49]:

$$\begin{cases} \theta_a(t) = k_1\theta_k(t) \\ k_1 = \dfrac{A_a}{A_k} \end{cases} \tag{6}$$

where $\theta_k(t)$ and $\theta_a(t)$ are the control signals of the knee and ankle joints at moment t, A_k and A_a are the absolute knee and ankle amplitudes, respectively, and k_1 is the absolute ankle–knee amplitude ratio. The knee–ankle mapping output signal is shown in Figure 6b.

With the legged robot motion mapping function, a single CPG neuron can realize the control of the whole leg, which simplifies the control process, reduces the computational complexity, and improves the control efficiency. In addition, the joint motion originating from animals is easier to integrate into the CPG control system, and the coordination of animal motion is inherited, which makes the motion of the legged robot closer to the real animal gait.

https://doi.org/10.1017/S0263574724001309 Published online by Cambridge University Press

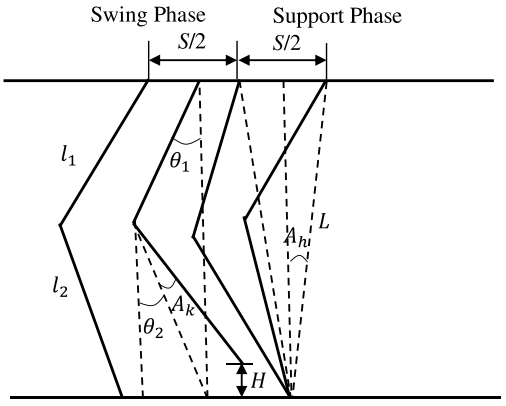


Figure 7. *Single-leg motion of a legged robot with a duty cycle of 1/2 kinematic gait.*

3.5. Setting of GD-CPG network parameters

There are many parameters in GD-CPG, and the determination of the parameter values needs to be combined with the structural characteristics of the legged robot itself and the characteristics of the motion gait. The magnitude of the CPG signal amplitude R_i determines the rotational range of the leg joints of the legged robot, taking the legged robot gait with a duty cycle of 1/2 as an example, assuming that the length of the thighs of the legged robot is l_1 and that the length of the legs is l_2, the length of the line between the root of the thigh and the end of the leg when it is in the support phase is L. The length of the line between the thigh's root and the calf's end is L when it is in the support phase. The single-cycle motion state of the single leg of the legged robot is shown in Figure 7, with thigh and knee oscillations of A_h and A_k, respectively, and the maximum height of the end of the foot off the ground of H, and the center of mass of the body moves forward by half a step length of $S/2$ in the support phase and swing phase, respectively. The angles between the thigh and calf and the vertical at the initial state are θ_1 and θ_2, respectively.

From Figure 7, we can get the legged robot thigh swing amplitude [50]:

$$A_h = \arcsin\left(\frac{S}{4L}\right) \tag{7}$$

Then generalize it to arbitrary gaits:

$$A_h = \arcsin\left(\frac{\beta S}{2(l_1 \cos\theta_1 + l_2 \cos\theta_2}\right) \tag{8}$$

where β is the gait duty cycle. From the thigh–knee mapping law, it can be obtained that the knee contraction is the largest when the leg is at the midpoint of the swing phase. At this time, the knee angle is the amplitude A_k, and the height of the end of the foot from the ground is H, from which the maximum height of the end of the foot from the ground can be obtained:

$$H = l_2 \cos\theta_2 - l_2 \cos(\theta_2 + A_k) \tag{9}$$

The knee amplitude can be calculated [50]:

$$A_k = \arccos\left(\frac{l_2 \cos\theta_2 - H}{l_2}\right) - \theta_2. \tag{10}$$

According to the GD-CPG model equations, the appropriate values of the CPG network parameters R_i can be derived from the structural parameters of the legged robot. However, due to the limitation of the control signal-sending frequency and other experimental conditions, the parameters need to be adjusted according to the actual control situation when conducting simulation and physical experiments.

The motion frequency of the legged robot can be controlled by adjusting the CPG signal frequency ω_i, which needs to be adjusted according to the actual control situation because the motion of each gait

https://doi.org/10.1017/S0263574724001309 Published online by Cambridge University Press

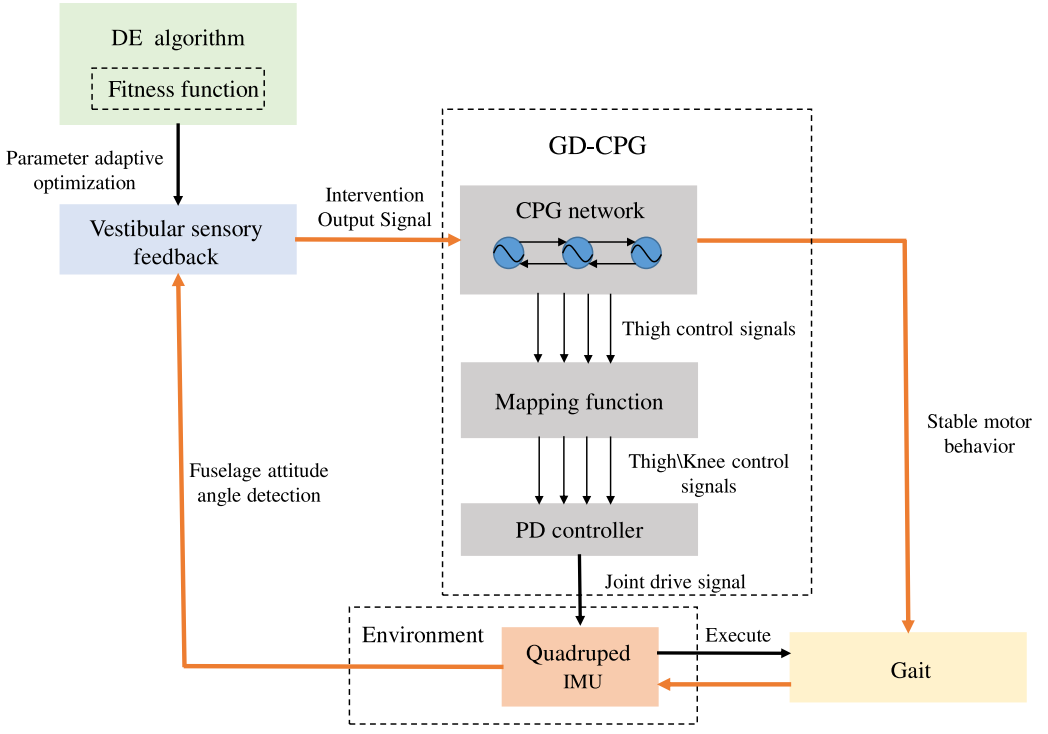


Figure 8. *RG-CPG control framework.*

is different. The C_i represents the bias of the CPG signal, which is usually set to 0. The a_i determines the convergence speed of the CPG signal, which is usually set to 2.0 according to experience, and the phase of each oscillator φ_i is adjusted within the range of 0 to 2π according to the typical characteristics of the legged robot's gaits.

4. RG-CPG-based motion control method for legged robots

The framework of the motion control method for the legged robot based on RG-CPG is shown in Figure 8. GD-CPG is the foundation of this section. As shown in the dotted box, the GD-CPG network model consists of three parts: the GD-CPG oscillator network generates the quadruped robot thigh joint drive signals, which are then converted to knee joint drive signals by the kinematic mapping function, and finally scaled to the actual joint input curves by the PD controller. However, such a controller can only meet the requirements of quadruped robots moving on smooth ground, and to enhance the ability of quadruped robots to cope with complex terrain, in this paper, the biological vestibular sensory feedback mechanism is modeled based on the GD-CPG model. The IMU sensors embedded in the body of the quadruped robot can provide real-time fuselage 3-axis attitude angle and serve as the input for vestibular feedback, which intervenes in the output of the CPG network to adjust the rotation range of the robot joints, and ultimately stabilizes the robot's motion behavior, to complete the feedback closed loop. Moreover, the DE algorithm is introduced and the corresponding fitness function is designed to complete the vestibular sensory feedback parameter adaptive optimization, which improves the control efficiency of the legged robot and further enhances the robot's motion performance. This section describes the implementation details of RG-CPG.

https://doi.org/10.1017/S0263574724001309 Published online by Cambridge University Press

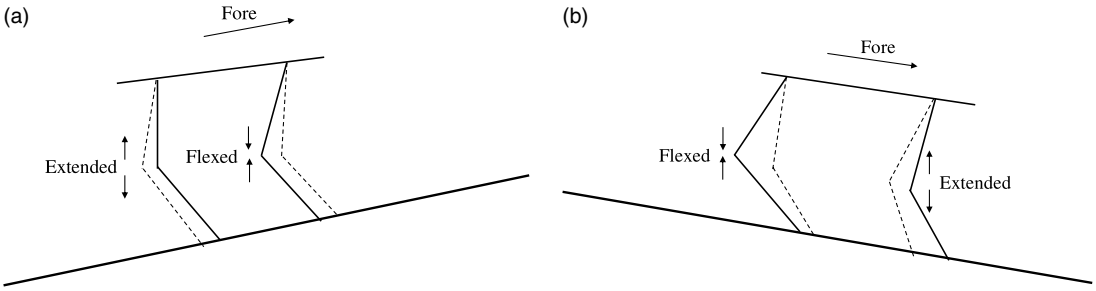


Figure 9. *Full-elbow quadruped in up-and-down slope. (a) Upslope, (b) Downslope.*

4.1. Vestibular sensory feedback

Quadruped robots may slip and tip over when moving on slopes and other complex terrains, which requires appropriate adjustment of body posture to maintain body balance. Vestibular sensory feedback refers to a kind of reflex behavior in which animals use vestibular organs to detect body posture, adjust muscle posture, and maintain the balance of the body during movement. Researchers can realize the function of quadruped robots moving on complex terrain with the help of biological vestibular sensory feedback.

Studies of slope movements in quadrupeds have found that they change the range of motion or equilibrium position of their front and rear legs to adjust their body posture to maintain body balance or reduce energy consumption under slope conditions. In the case of full-elbow quadrupeds, for example, when moving upslope, they adjust their body posture to low front and high rear, with the thigh and knee joints of the front legs flexed and the thigh and knee joints of the rear legs extended (as shown in Figure 9a); when moving downslope, their body posture is adjusted to high front and low rear, with the thigh and knee joints of the front legs extended and the thigh and knee joints of the rear legs flexed (as shown in Figure 9b).

Benefiting from the scalability of the GD-CPG model, combined with the sensory feedback of the quadruped robot interacting with the environment, the GD-CPG can generate adaptive control signals. Therefore, inspired by the vestibular sensory feedback mechanism of animals, this article models it in the GD-CPG model (Eq. (1)) and mimics the balance mechanism of body pitch angle by adding the balance functions of body roll angle and yaw angle:

$$\begin{cases} \dot{\varphi}_i = \omega_i + M\{i,:\} \cdot \Phi + N\{i,:\} \cdot \tilde{\Theta} \\ \ddot{r}_i = a_i \left[\dfrac{a_i}{4}(R_i - r_i) - \dot{r}_i \right] \\ \ddot{c}_i = a_i \left[\dfrac{a_i}{4}(C_i - c_i) - \dot{c}_i \right] \\ x_i = c_i + r_i \sin(\varphi_i) + feed_i \end{cases} \tag{11}$$

this article has added a vestibular feedback term named $feed_i$ to Eq. (1), which is computed from the body's three-axis attitude angles (pitch, roll, and yaw) obtained from the IMU's real-time measurements. It can be extended as

$$feed_i = \sigma_p(leg) \cdot k_p \theta_{pitch} + \sigma_r(leg) \cdot k_r \theta_{roll} + \sigma_y(leg) \cdot k_y \theta_{yaw} \tag{12}$$

where,

$$\sigma_p(leg) = \begin{cases} 1, & \text{RL or RR} \\ -1, & \text{FL or FR} \end{cases},$$

https://doi.org/10.1017/S0263574724001309 Published online by Cambridge University Press

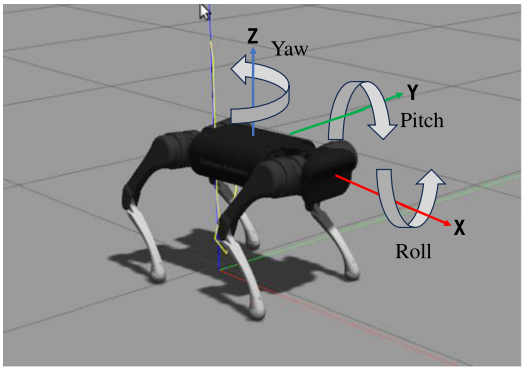


Figure 10. *Three-axis attitude angles of a quadruped robot body.*

$$\sigma_r(leg) = \begin{cases} -1, & \text{FR or RR} \\ 1, & \text{FL or RL} \end{cases},$$

$$\sigma_y(leg) = \begin{cases} -1, & \text{FL or RL} \\ 1, & \text{FR or RR} \end{cases}.$$

k_p, k_r, and k_y denote the body attitude gains, and θ_{pitch}, θ_{roll}, and θ_{yaw} denote the quadruped robot body pitch, roll, and yaw angles (shown in Figure 10).

At this point, the knee joint makes a reverse isometric rotation relative to the thigh joint of the same leg:

$$\theta_{k_1} = \theta_{k_0} - (\theta_{t_1} - \theta_{t_0}) \tag{13}$$

where,θ_{k_1}, θ_{t_1}, θ_{k_0}, and θ_{t_0} denote the knee and thigh angular positions adjusted by the vestibular sensory feedback as well as the pre-adjusted knee and thigh angular positions, respectively.

From Eqs. (12) and (13), it can be seen that this article uses the method of reversing the change of rotational equilibrium position of the front and rear legs to adaptively adjust the kinematic attitude of the quadruped robot when going up and down the slope. When going upslope, the front leg thigh joint equilibrium position is shifted backward and the rear leg thigh joint equilibrium position is shifted forward. The knee joint makes a reverse equirectangular rotation relative to the thigh joint of the same leg, keeping the absolute attitude in knee space unchanged. After adjusting the quadruped robot, the front leg is flexed, the rear leg is extended, and the body attitude becomes low in the front and high in the rear; when going downslope, the balance position of the thigh joint of the front leg is shifted forward, and the balance position of the thigh joint of the rear leg is shifted rear. The knee joint changes accordingly. After adjustment, the quadruped robot's front leg is extended, the rear leg is flexed, and the body attitude becomes high in the front and low in the rear. When the body of the quadruped robot moves sideways or deviates from the desired direction, the changes in the roll angle and yaw angle will also trigger the vestibular sensory feedback mechanism to adjust the motion behavior of the quadruped robot.

4.2. DE algorithm

To stabilize the motion of the quadruped robot in complex terrain and make the robot reach a better motion state quickly, the setting of the magnitude of the attitude angle gain of each body in the vestibular sensory feedback mechanism needs to be considered comprehensively. In Eq. (12), the relationship

https://doi.org/10.1017/S0263574724001309 Published online by Cambridge University Press

between vestibular sensory feedback gains k_p, k_r and k_y is not clear, and the use of observation or trial-and-error method to adjust the parameter needs to spend a lot of time with little effect. To address this problem, this article introduces the DE algorithm to adaptively optimize the vestibular sensory feedback parameters of the quadruped robot, so that the quadruped robot quickly reaches a better motion state and improves the control efficiency.

4.2.1. Algorithmic implementation

The DE algorithm is a stochastic heuristic search algorithm based on group intelligence. It was proposed in 1995 by Rainer Storn and Keneth Price [51]. The DE algorithm retains the population-based global search strategy with strong global convergence and robustness by using real number coding, simple difference-based mutation operations, and a one-to-one competitive survival strategy.

The basic structure of the DE algorithm is similar to other evolutionary algorithms and consists of three basic operations: mutation, crossover, and selection. The DE algorithm introduced in this article consists of the following four steps [52]:

1. Generating the initial population: Randomly generate N individuals in d-dimensional space that satisfy the constraints:

$$x_{ij}(0) = \text{rand}_{ij}(0, 1)(x_{ij}^U - x_{ij}^L) + x_{ij}^L \tag{14}$$

   where x_{ij}^U and x_{ij}^L are the upper and lower bounds of the jth chromosome, respectively, and $\text{rand}_{ij}(0, 1)$ is a random decimal between [0, 1].

2. Mutation: Three individuals x_{p1}, x_{p2} and x_{p3} with $i \neq p_1 \neq p_2 \neq p_3$ are randomly selected from the population for mutation:

$$h_{ij}(t+1) = x_{p_1 j}(t) + F(x_{p_2 j}(t) - x_{p_3 j}(t)) \tag{15}$$

   where $x_{p_2 j}(t) - x_{p_3 j}(t)$ is the vector difference, F is the scaling factor, and p_1, p_2, and p_3 are random integers that identify individuals in the population.

3. Crossover: Crossover is designed to increase the diversity of populations:

$$v_{ij}(t+1) = \begin{cases} h_{ij}(t+1), & \text{rand } l_{ij} \leq CR \\ x_{ij}(t), & \text{rand } l_{ij} > CR \end{cases} \tag{16}$$

   where rand l_{ij} is a random decimal between [0, 1], CR is the crossover probability, and $CR \in [0, 1]$.

4. Selection: The fitness values of the test vector $v_i(t+1)$ and the target vector $x_i(t)$ are compared to determine the members of the next generation of the population:

$$x_i(t+1) = \begin{cases} v_i(t+1), & f(v_{i1}(t+1), \ldots, v_{in}(t+1)) > f(x_{i1}(t), \ldots, x_{in}(t)) \\ x_{ij}(t), & f(v_{i1}(t+1), \ldots, v_{in}(t+1)) \leq f(x_{i1}(t), \ldots, x_{in}(t)) \end{cases} \tag{17}$$

Loop through the steps 2–4 operations until the maximum number of evolutionary generations G is reached.

4.2.2. Motion fitness function

The purpose of optimizing vestibular sensory feedback parameters using DE algorithms is to maximize the kinematic performance enhancement of the quadruped robot in the shortest possible time and improve control efficiency. To quantify the motion performance of the quadruped robot, this article designs the motion fitness function of the quadruped robot, which is based on the motion stability and movement speed of the quadruped robot:

$$Fitness = \bar{V} \times \nabla_P \times \nabla_R \times \nabla_Y \tag{18}$$

https://doi.org/10.1017/S0263574724001309 Published online by Cambridge University Press

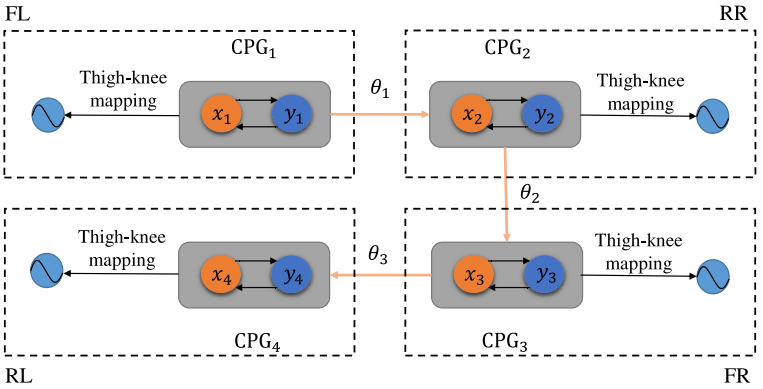


Figure 11. *Motion control system for the quadruped robot based on GD-CPG.*

where,

$$\nabla_P = \left(\frac{1}{1 + \frac{1}{\tau} \sum_{t=0}^{\tau} |\theta_P(t)|} \right)^{\beta_P} \tag{19}$$

$$\nabla_R = \left(\frac{1}{1 + \frac{1}{\tau} \sum_{t=0}^{\tau} |\theta_R(t)|} \right)^{\beta_R} \tag{20}$$

$$\nabla_Y = \left(\frac{1}{1 + \frac{1}{\tau} \sum_{t=0}^{\tau} |\theta_Y(t)|} \right)^{\beta_Y} \tag{21}$$

In the above equations, $\bar{V}$ is the average velocity of the quadruped robot during its motion, and ∇_P, ∇_R, and ∇_Y are the angular gain of the attitude of the body of the quadruped robot during its motion. $\theta_P(t)$, $\theta_R(t)$, and $\theta_Y(t)$ are the pitch, roll, and yaw angles of the robot body at time t, τ is the simulation time, and β_P, β_R, and β_Y are coefficients used to minimize attitude angle. Priority is given to the maximization of the moving speed by changing the size of this coefficient. The optimization of the motion performance of quadruped robots with different focuses can be achieved. This paper usually set $\beta_P = \beta_R = \beta_Y = 1$.

In summary, the role of the fitness function proposed in this article is to maximize the moving speed of the quadruped robot as well as minimize the range of changes in the body attitude angle during the iteration process, to enhance the kinematic performance of the quadruped robot.

5. Simulation and analysis

This section will verify the validity, robustness, and transferability of GD-CPG through legged robot gait simulations and gait continuous transition simulations; verify the validity of RG-CPG through slope simulation; and highlight the superiority of RG-CPG through comparison simulations with other existing CPG models

5.1. Simulations on gait motion of the quadruped and hexapod robots

5.1.1. Simulations on three-gait and continuous transitions of the quadruped robot

The quadruped robot control system in this simulation is shown in Figure 11, which uses four oscillator-coupled GD-CPG neural networks to generate four periodic signals to drive the quadruped robot's thigh joint motion, and then generates the corresponding knee drive signals through the thigh–knee mapping

https://doi.org/10.1017/S0263574724001309 Published online by Cambridge University Press

Table I. *Gait parameter setting for quadruped robot GD-CPG.*

Parameters	ω_i	R_i	C_i	a_i	φ_1	φ_2	φ_3	φ_4
Walking gait	$\frac{\pi}{20}$	1.05	0	2.0	0	$\frac{\pi}{2}$	π	$\frac{3\pi}{2}$
Trotting gait	$\frac{\pi}{22.5}$	2.55	0	2.0	0	0	π	π
galloping gait	$\frac{\pi}{20}$	1.35	0	2.0	0	π	0	π

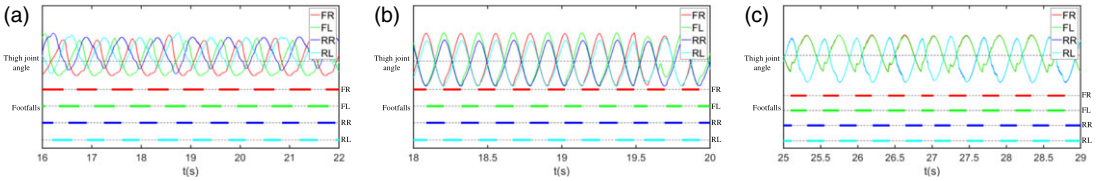


Figure 12. *Motion state diagram of the quadruped robot in three gait states. (a) Walking gait, (b) Trotting gait, (c) Galloping gait.*

function, thus completing the motion control of the quadruped robot. Finally, the parameters of the CPG network are adjusted to make the quadruped robot accomplish different gait movements.

In this simulation, a GD-CPG-based quadruped robot is controlled to execute walking, trotting, and galloping gaits. The GD-CPG parameters in the simulation were set as shown in Table I.

The motion state of the quadruped robot in the simulation is shown in Figure 12. For the thigh angle change curve in figure, the ascending phase represents the support phase and the descending phase represents the swing phase; for the footfall line segment, the colored thick solid line represents the support phase and the thin black dashed line represents the swing phase.

For the walking gait, during the simulation time, each leg of the quadruped robot touches the ground in turn and moves with the phase sequence FL – RR – FR – RL. This is a typical walking gait; for the trotting gait, the diagonal lateral legs of the quadruped robot constitute one set of alternating ground-contacting motion with the other set during the simulation time, with the phase sequence (FL, RR) – (FR, RL). This is a typical trotting gait; for the galloping gait, during the simulation time, the front and rear sets of legs of the quadruped robot alternately contacted the ground in motion with the phase sequence (FL, FR) – (RL, RR). This is a typical galloping gait. It can be concluded that the thigh–knee joint motion relationship of the quadruped robot based on GD-CPG is by the limb motion law of quadruped animals, and the curve is relatively smooth without cusp and mutation, which indicates that the limb motion relationship is more coordinated. Because the knee joint lifts the leg quickly and lands slowly, the swing leg does not easily rub the ground. The quadruped robot suffers less ground impact and is suitable for walking in all gaits.

In summary, the quadruped robot based on GD-CPG can complete the three gait motions of walking, trotting, and galloping in the simulation environment, which verifies the validity of GD-CPG for the control of quadruped robots.

The gait conversion discussed in this article mainly utilizes the dynamic characteristics of GD-CPG to realize different gaits by changing the network parameters, such as frequency and phase, to obtain multiple periodic signals with different phase relations. Completing the gait transition requires the quadruped robot to change the motion state in a short time, which requires high fault tolerance and robustness of the control system. In this article, a three-gait continuous transition simulation is designed based on the three-gait motion simulation. In this simulation, the quadruped robot based on GD-CPG executes several cycles of walking, trotting, and galloping gaits in sequence.

The state changes of the quadruped robot in the simulation are shown in Figure 13, where the quadruped robot moves in a walking gait between time $t = 43$ s and $t = 56.5$ s; in a trotting gait between time $t = 58$ s and $t = 63$ s; and in a galloping gait between time $t = 65$ s and $t = 73$ s. From Figure 13a, it can be seen that at the gait transition, the thigh angle curve re-stabilizes after about 2 s of fluctuation. It

https://doi.org/10.1017/S0263574724001309 Published online by Cambridge University Press

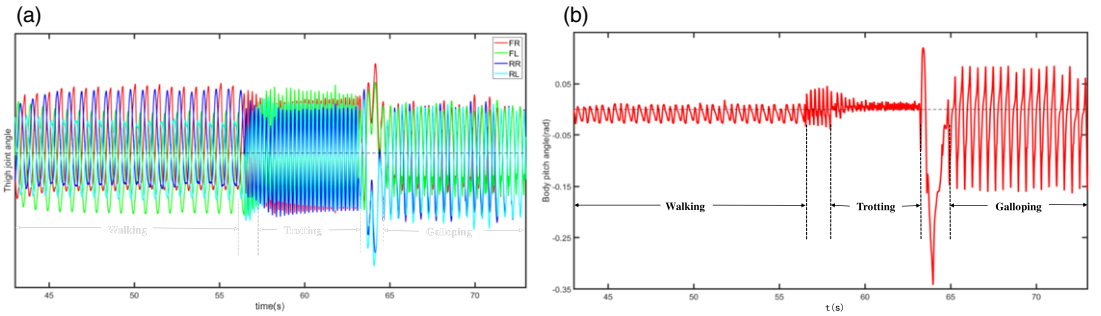


Figure 13. *Motion state diagram of the quadruped robot with three consecutive gait transitions. (a) Thigh angle change, (b) Body pitch angle change.*

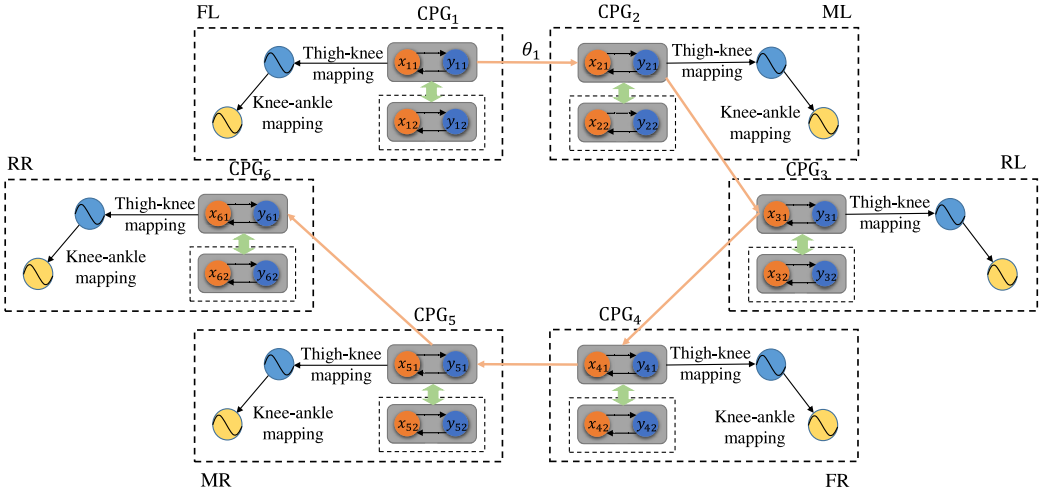


Figure 14. *Motion control system for the hexapod robot based on GD-CPG and BI-GD-CPG fitting.*

can be concluded that the quadruped robot based on GD-CPG can complete the transitions of different motion gaits in about 2 s. In addition, from Figure 13b, it can be seen that during the conversion of the quadruped robot from walking to trotting, the fluctuation of the change in the body pitch angle is relatively small, ranging from about 0.08 rad. However, during the transition from trotting to galloping, the change in body pitch angle fluctuates more, reaching 0.43 rad, which is caused by the fact that the front and rear legs of the quadruped robot contact the ground alternately during the execution of galloping gait, and the robot as a whole is in a forward and backward undulating state.

In summary, the quadruped robot quickly recovers to a stable state after a short period of irregular undulation of the body during the gait transition. It is demonstrated that the quadruped robot based on GD-CPG can complete the three gait transitions in the simulation environment, and the robustness of the GD-CPG control method is verified.

5.1.2. Simulations on three-gait locomotion of the hexapod robot

In this simulation, the control system of the hexapod robot is shown in Figure 14, when executing the tripod gait, the GD-CPG neural network coupled with six oscillators is used as the controller; when executing the tetrapod and wave gait, it is switched to the CPG neural network coupled with six BI-GD-CPG fitting oscillators. The six periodic signals generated by the CPG neural network drive the thigh joints of the hexapod robot, and then the corresponding knee and ankle drive signals are generated by

https://doi.org/10.1017/S0263574724001309 Published online by Cambridge University Press

Table II. *Gait parameter setting for hexapod robot GD-CPG.*

Parameters	ω_i	ω_p	ω_q	R_i	C_i	a_i	φ_1	φ_2	φ_3	φ_4	φ_5	φ_6
Tripod gait	$\frac{\pi}{10}$	–	–	5.7	0	2.0	0	π	0	π	0	π
Tetrapod gait	–	$\frac{\pi}{10}$	$\frac{\pi}{20}$	5.7	0	2.0	0	$\frac{2\pi}{3}$	$\frac{4\pi}{3}$	$\frac{4\pi}{3}$	0	$\frac{2\pi}{3}$
Wave gait	–	$\frac{\pi}{10}$	$\frac{\pi}{50}$	5.7	0	2.0	0	$\frac{\pi}{3}$	$\frac{2\pi}{3}$	π	$\frac{4\pi}{3}$	$\frac{5\pi}{3}$

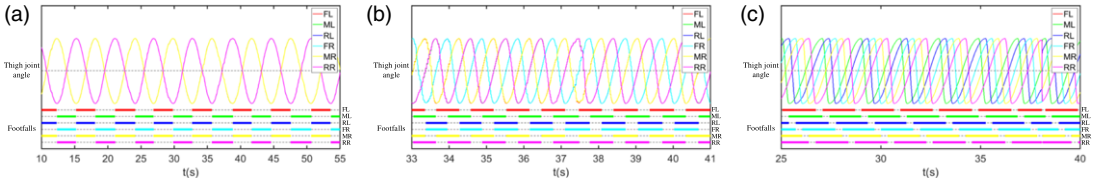


Figure 15. *Motion state diagram of the hexapod robot in three gait states. (a) Tripod gait, (b) Tetrapod gait, (c) Wave gait.*

the thigh–knee mapping function and the knee–ankle mapping function to complete the motion control of the hexapod robot. Finally, the parameters of the CPG network are adjusted to make the hexapod robot accomplish different gait movements.

In this simulation, the hexapod robot is controlled to execute tripod, tetrapod, and wave gaits. The GD-CPG parameters are set as shown in Table II.

The motion state of the hexapod robot in the simulation is shown in Figure 15. Since the model sets the counterclockwise rotation of the thigh joint as positive rotation and the clockwise rotation as negative rotation, for the right leg thigh joints (FR, MR, RR) of the body, the rising phase of the position curve is the swing phase and the falling phase is the support phase, and the signals should be flipped along the x-axis when inputting the control signals. To make the results intuitive, the subsequent simulation contents of this article will all show the position change curve of the right leg-thigh joint after flipping again. In summary, for the thigh joint angle change curve in the motion state diagram, the rising phase represents the support phase and the falling phase represents the swing phase; for the line segment of the landing point, the colored thick solid line represents the support phase and the black thin dashed line represents the swing phase.

For the tripod gait, the two sets of legs of the hexapod robot moved sequentially in alternating triangular contact with the ground during the simulation time, with the phase sequence (FL, RL, MR) – (FR, RR, ML). This is a typical tripod gait; for the tetrapod gait, the hexapod robot's oppositely asymmetric three sets of legs sequentially contacted the ground during the simulation time and moved in the phase sequence (FL, MR) – (ML, RR) – (RL, FR). This is a typical tetrapod gait; for the wave gait, during the simulation time, the six legs on both sides of the body of the hexapod robot moved in wave-like contact with the ground in sequence, and the phase sequence was FL – ML – RL – FR – MR – RR. This is a typical wave gait.

In summary, the hexapod robot based on GD-CPG and BI-GD-CPG fitting can accomplish the three gait mtotions of tripod, tetrapod, and wave in the simulation environment, which verifies the validity and ransferability of the GD-CPG control method.

5.2. Simulation on adaptive optimization of vestibular sensory feedback parameters

In this simulation, the RG-CPG-based quadruped robot is controlled to execute walking, trotting, and galloping gaits in a simulation environment, and the vestibular sensory feedback gains k_p, k_r, and k_y in Eq. (12) are adaptively optimized in the process, and parameter settings of the DE algorithm are shown in Table III.

https://doi.org/10.1017/S0263574724001309 Published online by Cambridge University Press

Table III. *Parameter setting for DE algorithm.*

Parameters	Values
Scaling factor F	3.0
Crossing probability CR	0.9
Evolutionary generations G	70
Population size N	30

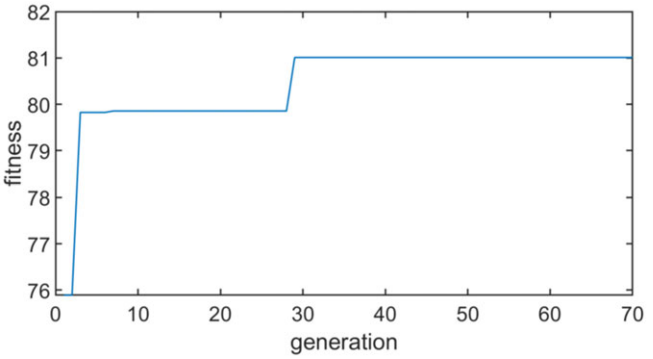


Figure 16. *Fitness value changes during the execution of walking gait by the quadruped robot.*

Figure 16 shows the algorithm iterations during the execution of the walking gait by the quadruped robot. As can be seen from the figure, prior to the optimization of the DE algorithm, the kinematic fitness function (kinematic performance score) of the quadruped robot was 76 or less when using randomly searched vestibular sensory feedback parameters, after 70 rounds of iterations, the fitness value is finally stabilized above 80. This suggests that vestibular sensory feedback parameters optimized by DE algorithms can enhance the locomotor performance of quadruped robots. The optimized vestibular sensory feedback parameters for the three gaits of the quadruped robot are shown in Table IV. In this article, these parameters will be used in the next experiments for RG-CPG-based motion control of quadruped robots.

5.3. Slope simulation

To test the ability of the RG-CPG-based quadruped robot to cope with complex terrain, this article designs the slope terrain simulation. In the simulation, the simulation environment is a bounded 3D region in which a symmetric slope device is set up. As shown in Figure 17, this slope device consists of an upslope section, a platform at the top of the slope, and a downslope section, with an inclination of 11° and a width of 0.5 m. The simulation sets the RG-CPG-controlled quadruped robot to pass through the slope device in trotting and galloping gaits, respectively, and the parameters of the two gaits for the RG-CPG are set as shown in Table V.

Figure 18 shows a snapshot of the quadruped robot passing through the slope device during the simulation. This article records the motion state of the quadruped robot during the simulation, as shown in Figure 19, with the colored curves at the top representing the change in the angle of each thigh joint, and since the change in the pitch angle of the robot's body is most pronounced during the slope movement, this article plots the change in the pitch angle of the body represented by the black curve at the bottom. For the trotting gait, it can be seen from Figure 19a that the robot is in the upslope phase between $t = 83$s and $t = 86.2$ s. At this time, the robot body is tilted backward (the pitch angle decreases), the thigh joint angles of the left front leg (FL) and the right front leg (FR) increase, and the whole leg is

https://doi.org/10.1017/S0263574724001309 Published online by Cambridge University Press

Table IV. *Vestibular sensory feedback parameters of the quadruped robot optimized by DE algorithm.*

Parameters	walking gait	trotting gait	galloping gait
k_p	0.62	0.81	0.93
k_r	0.31	0.45	0.39
k_y	0.16	0.12	0.28

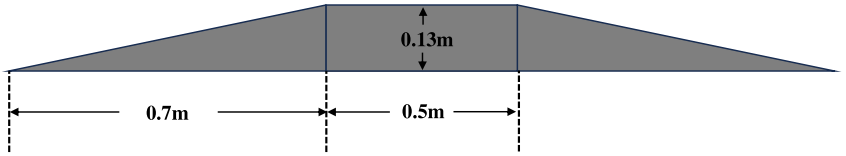


Figure 17. *Slope device.*

flexed, the thigh joint angles of the left rear leg (RL) and the right rear leg (RR) decrease, and the whole leg is extended, and the robot overall presents a low front and high rear attitude, similar to the one in Figure 9a. Between $t = 86.2$ s and $t = 87.6$ s, the robot moves at the platform at the top of the slope. At this time, the robot's front and rear leg joint angles change consistently, showing a standard trotting gait. Between $t = 87.6$ s and $t = 89.5$ s, the robot was in the downslope phase. At this time, the robot body is tilted forward (the pitch angle increases), the thigh joint angles of the left front leg (FL) and the right front leg (FR) decrease, and the whole leg is extended, the thigh joint angles of the left rear leg (RL) and the right rear leg (RR) increase, and the whole leg is flexed, and the robot has a high front and low rear attitude, similar to the one in Figure 9b. For the galloping gait, it can be seen from Figure 19b that the robot is in the upslope phase between $t = 14$ s and $t = 19.5$ s. Between $t = 19.5$ s and $t = 22.3$ s, the robot is moving on the platform at the top of the slope. Between $t = 22.3$ s and $t = 25$ s, the robot is in the downslope phase. The state changes of the robot body and each thigh joint during this period are similar to the trotting gait.

In summary, the quadruped robot based on RG-CPG can adjust the joint rotation angle in real time to pass through unstructured terrain with a straight-line motion in a complex environment. In the simulation, the quadruped robot passes through the slope device with a slope of 11° in a straight line with trotting and galloping gaits, which verifies the validity of the RG-CPG control method.

5.4. Comparative simulations with other CPG control methods

To reveal the superiority of the RG-CPG control method, this section compares the RG-CPG control method with the more popular Matsuoka-CPG control method and the GD-CPG control method.

In this simulation, programs are written based on Matsuoka-CPG, GD-CPG, and RG-CPG to control the quadruped robot to execute walking gait and galloping gait along the positive direction of x-axis, respectively. Then, the motion control performances of the three CPG models for the quadruped robot were compared in terms of stability, linear motion capability, speed, and overall motion performance, respectively. In the simulation, each CPG output signal frequency, amplitude, offset value, and joint drive signal sending frequency are the same. The parameter settings of GD-CPG and RG-CPG are given in Tables VI and VII.

During the motion of a quadruped robot, if the body tilt angle is larger, the robot motion is more unstable, and vice versa, it means the motion is more stable. So in the simulation, the size of the range of variation of the pitch and roll angles of the quadruped robot body represents the degree of stabilization of the robot motion. For the walking gait, Figure 20 shows the angular variation of pitch and roll angles during the motion of the quadruped robot under different CPG controls. It can be seen that the Matsuoka-CPG-based quadruped robot performs walking gait with pitch angle variations ranging

https://doi.org/10.1017/S0263574724001309 Published online by Cambridge University Press

Table V. *Slope simulation RG-CPG parameter setting.*

Parameters	ω_i	R_i	C_i	a_i	φ_1	φ_2	φ_3	φ_4	k_p	k_r	k_y
Trotting gait	$\frac{\pi}{17.5}$	2.78	0	2.4	0	0	π	π	0.81	0.45	0.12
Galloping gait	$\frac{\pi}{16}$	1.56	0	2.4	0	π	0	π	0.93	0.39	0.28

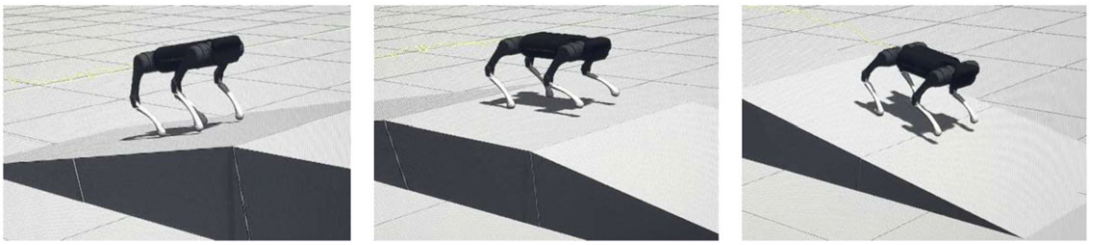


Figure 18. *Snapshots of the quadruped robot going upslope (left), platform motion (center), and downslope (right).*

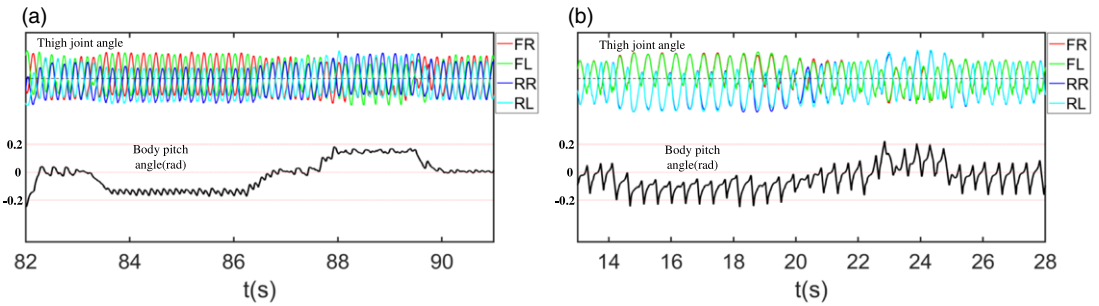


Figure 19. *Quadruped robot going up and down a slope. (a) Trotting gait, (b) Galloping gait.*

from –0.044 rad to 0.011 rad and roll angle variations ranging from –0.081 rad to 0.080 rad, while the GD-CPG-based quadruped robot performs motion with pitch angle variations ranging from –0.027 rad to 0.012 rad, and the roll angle variations ranging from –0.069 rad to 0.063 rad; while for the RG-CPG-based quadruped robot, the ranges of these two metrics are –0.011 rad to 0.008 rad and –0.027 rad to 0.028 rad, respectively, which are both better than the Matuoka-CPG and GD-CPG results. For the galloping gait, Figure 21 shows the angular changes of pitch and roll angles during the motion of the quadruped robot under different CPG controls. It can be seen that the pitch angle of the Matsuoka-CPG-based quadruped robot varies from –0.134 rad to 0.130 rad and the roll angle varies from –0.015 rad to 0.011 rad during the execution of the galloping gait; the pitch angle of the GD-CPG-based quadruped robot varies from –0.720 rad to –0.150 rad, and the variation range of roll angle is –0.008 rad to 0.004 rad; while for the RG-CPG-based quadruped robot, the ranges of these two metrics are –0.165 rad to 0.080 rad and –0.010 rad to 0.007 rad, respectively. Compared to the Matsuoka-CPG and GD-CPG, the RG-CPG-controlled quadruped robot adjusts the joint rotation ranges by vestibular sensory feedback mechanism to reduce the size of the range of variation of the pitch and roll angles of the body during the motion to improve the comprehensive stability of the motion. The simulation results show that the RG-CPG-based quadruped robot has a more stable body during the execution of walking and galloping gaits.

The yaw angle of the body of the quadruped robot reflects the actual motion direction of the robot during the motion process, and in this simulation, the closer the yaw angle of the body is to 0 rad indicates that the robot moves better along the positive direction of the x-axis. Figure 22a shows the change of yaw angle during the execution of the walking gait of the quadruped robot under three kinds of CPG control.

https://doi.org/10.1017/S0263574724001309 Published online by Cambridge University Press

Table VI. *GD-CPG parameter setting in comparative simulations.*

Parameters	ω_i	R_i	C_i	a_i	φ_1	φ_2	φ_3	φ_4
Walking gait	$\frac{\pi}{20}$	1.05	0	2.0	0	$\frac{\pi}{2}$	π	$\frac{3\pi}{2}$
Galloping gait	$\frac{\pi}{22.5}$	1.35	0	2.0	0	π	0	π

Table VII. *RG-CPG parameter setting in comparative simulations.*

Parameters	ω_i	R_i	C_i	a_i	φ_1	φ_2	φ_3	φ_4	k_p	k_r	k_y
Walking gait	$\frac{\pi}{20}$	1.05	0	2.0	0	$\frac{\pi}{2}$	π	$\frac{3\pi}{2}$	0.62	0.31	0.16
Galloping gait	$\frac{\pi}{22.5}$	1.35	0	2.0	0	π	0	π	0.93	0.39	0.28

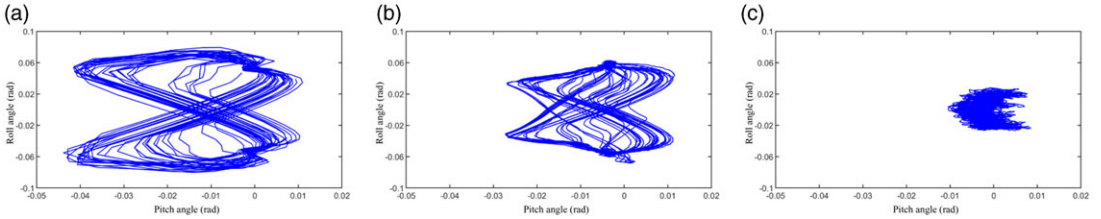


Figure 20. *Pitch and roll angle change during the execution of walking gait by the quadruped robot based on three CPG models. (a) Matsuoka-CPG, (b) GD-CPG, (c) RG-CPG.*

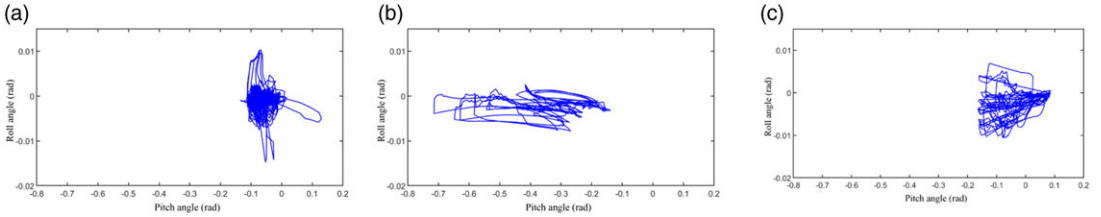


Figure 21. *Pitch and roll angle change during the execution of galloping gait by the quadruped robot based on three CPG models. (a) Matsuoka-CPG, (b) GD-CPG, (c) RG-CPG.*

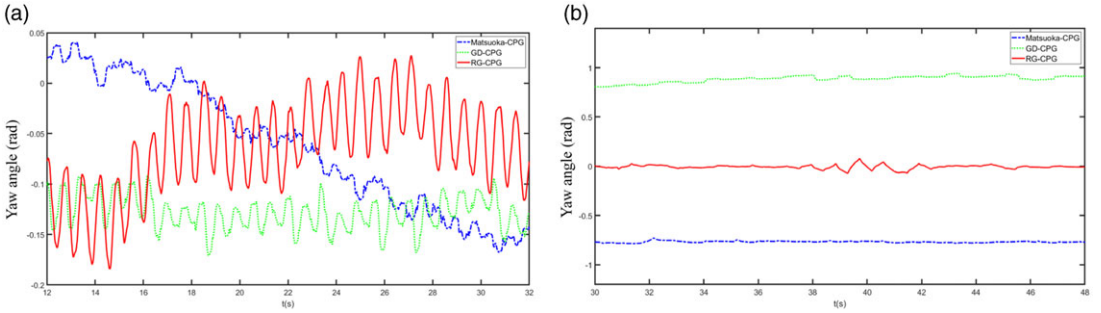


Figure 22. *Comparison of yaw angle changes during quadruped robot motion based on three CPG models. (a) Walking gait, (b) Galloping gait.*

https://doi.org/10.1017/S0263574724001309 Published online by Cambridge University Press

From the figure, we can see that the yaw angle of the body of the Matsuoka-CPG-based quadruped robot decreases continuously during motion, representing that the forward direction of the robot gradually shifts to the negative direction of the y-axis (relative to the right of the positive direction of the x-axis) during motion; whereas, the yaw angle of the body of the GD-CPG-based quadruped robot is always maintained at around –0.13 rad during motion, which means that the robot always moves in the negative direction of the y-axis compared to the desired motion; while the yaw angle of the quadruped robot based on RG-CPG is around –0.13 rad from $t = 12$ s to $t = 15$ s, which means that the robot's motion direction is biased in the negative direction of the y-axis during this period. After that, the body yaw angle gradually approaches 0 rad, indicating that the quadruped robot gradually adjusts its motion direction towards the desired motion under the intervention of the vestibular sensory feedback mechanism. For the galloping gait, it can be seen from Figure 22b that the yaw angle of the body of the Matsuoka-CPG-based quadruped robot is maintained at around –0.75 rad during the motion, indicating that the robot is substantially biased towards the negative direction of the y-axis compared to the desired motion; while the yaw angle of the body of the GD-CPG-based quadruped robot is maintained at 0.8 rad during the motion, indicating that the robot moves in the positive direction of the y-axis (left relative to the positive direction of the x-axis); the yaw angle of the body of the quadruped based on RG-CPG stays stable around 0 rad from $t = 30$ s to $t = 37$ s, which means that the robot moves in the positive direction of the x-axis during this period (the desired motion); between $t = 37$ s and $t = 42$ s, the yaw angle fluctuates upward and downward, indicating that the robot has been disturbed by some kind of interference during this period, resulting in a left-right biased motion. After that, the yaw angle of the body quickly returned to 0 rad, meaning that the quadruped robot quickly changed its forward direction and recovered the desired motion by adjusting its motion state with the intervention of the vestibular sensory feedback mechanism. The simulation results show that the quadruped robot based on RG-CPG can adjust the motion state in real time according to the actual situation during the motion process to better accomplish the linear motion.

Motion speed is also an important index to measure the robot's motion ability. Since the quadruped robot is set to move at a constant rate in this simulation, the real-time motion velocity of the quadruped robot is intercepted in this article for the simulation. Figure 23a shows the comparison of the motion speed along the positive direction of the x-axis during the execution of the walking gait of the quadruped robot under the control of the three CPGs, the motion speed along the positive direction of the x-axis during the motion of the quadruped robot based on the Matsuoka-CPG is 0.073 m/s; the quadruped robot based on the GD-CPG has a motion speed of 0.096 m/s; and 0.132 m/s for the RG-CPG-based quadruped, which is higher than the results of the other two; for the galloping gait, it can be seen from Figure 23b that the Matsuoka-CPG-based quadruped robot moves at about 0.194 m/s in the positive direction of the x-axis during motion; the GD-CPG-based quadruped robot has a metric of 0.119 m/s; the RG-CPG-based quadruped robot has a metric of 0.437 m/s, which is higher than the results of the other two. The simulation results show that the RG-CPG-based quadruped robot moves faster during the execution of walking and galloping gaits under the same conditions.

To compare the integrated motion performance of the quadruped robots under the control of the three CPGs and to quantify the advantages of RG-CPG, this article calculates the fitness values of the motion of the quadruped robots under the control of the Matsuoka-CPG, the GD-CPG, and the RG-CPG, respectively, based on the fitness function in Eq. (18) and compares them. As shown in Figure 24, the integrated motion performance of the quadruped robot based on RG-CPG executing walking gait is improved by about 87.9% compared to Matsuoka-CPG, and 49.24% compared to GD-CPG; the integrated motion performance of the RG-CPG-based quadruped robot in performing galloping gait is improved by about 228.36% over Matsuoka-CPG and 609.68% over GD-CPG.

In summary, compared with Matsuoka-CPG and GD-CPG, the quadruped robot controlled by RG-CPG demonstrated better stability, linear motion capability, and speed in executing walking and galloping gaits, and the advantages in terms of integrated motion performance were more obvious, which verified the superiority of the RG-CPG control method.

https://doi.org/10.1017/S0263574724001309 Published online by Cambridge University Press

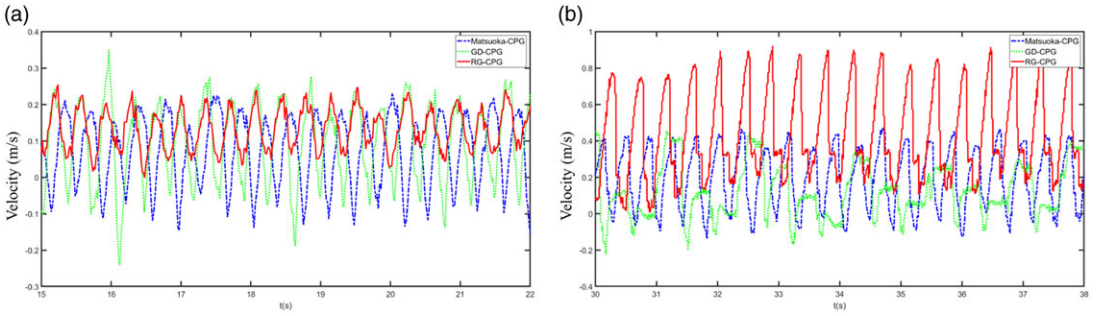


Figure 23. *Comparison of motion velocity during quadruped robot motion based on three CPG models. (a) Walking gait, (b) Galloping gait.*

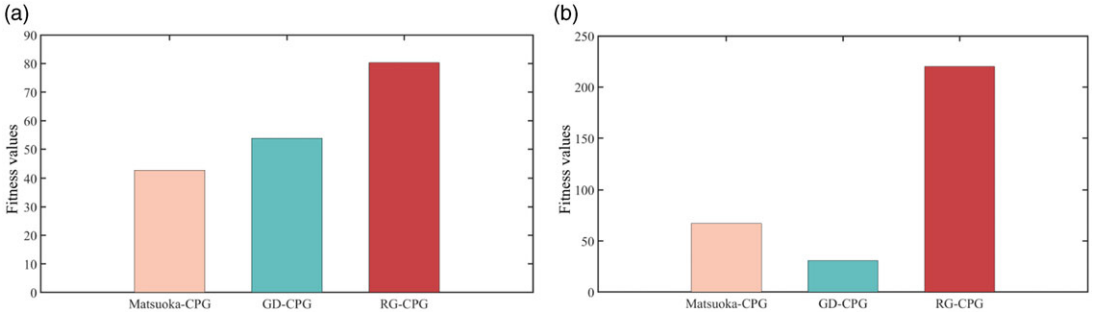


Figure 24. *Comparison of integrated motion performance of quadruped robots based on three CPG models. (a) Walking gait, (b) galloping gait.*

6. Physical experiments

In this section, legged robot gait experiments in the real world are designed based on existing legged robot experiment platforms to verify the feasibility of the GD-CPG control method in the real world.

6.1. Experiment based on the quadruped robot

The quadruped robot control system consists of a control board, servo motors, batteries, sensors, and control software. The technical specifications are shown in Table VIII.

This experiment is based on GD-CPG to write a program to control the quadruped robot to perform walking and trotting gait. The experiment sets the equilibrium positions of the thigh and knee joints of the quadruped robot to be 1.2 rad and –2.0 rad, respectively, and the rotation of the joints towards the rear of the body is considered positive rotation, and vice versa is considered negative rotation. The parameter settings of the GD-CPG are shown in Table IX.

Figures 25 and 26 show the thigh and knee joint angle changes and experimental snapshots of each leg during the execution of the walking gait of the quadruped robot, respectively. From Figure 25a, it can be seen that the thigh joint angle varies from 1.05 rad to 1.35 rad during the motion of the quadruped robot. The waveforms are relatively smooth, indicating smooth motion, and are symmetric along the equilibrium position of the thigh joint, which is a standard symmetry-like sine wave. The knee joint (Figure 25b) shows a half-wave in the swing phase, with a maximum angle of rotation of about -2.25 rad. The curve is smooth, indicating smooth rotation in the swing phase; the knee joint is slightly out of the equilibrium position in the support phase, and it is more pronounced in the knee joints of the rear legs (RR and RL), reaching about -2.1 rad. The reason is that the center of mass of the quadruped robot

https://doi.org/10.1017/S0263574724001309 Published online by Cambridge University Press

Table VIII. *Technical specifications of the quadruped robot.*

Parameters	**Values**
Size	1126 × 467 × 636mm
Weight	50 kg
Thigh range of rotation	−1.0∼3.5 rad
Knee range of rotation	−2.6∼-0.6 rad
Maximum instantaneous torque of joints	210 N.m
Main controller CPU	Intel i5-1135G7
Operating system	Ubuntu

Table IX. *GD-CPG parameter setting for the quadruped robot.*

Parameters	ω_i	R_i	C_i	a_i	φ_1	φ_2	φ_3	φ_4
Walking gait	$\frac{\pi}{20}$	1.575	0	2.0	0	$\frac{\pi}{2}$	π	$\frac{3\pi}{2}$
Trotting gait	$\frac{\pi}{18.5}$	1.426	0	2.0	0	0	π	π

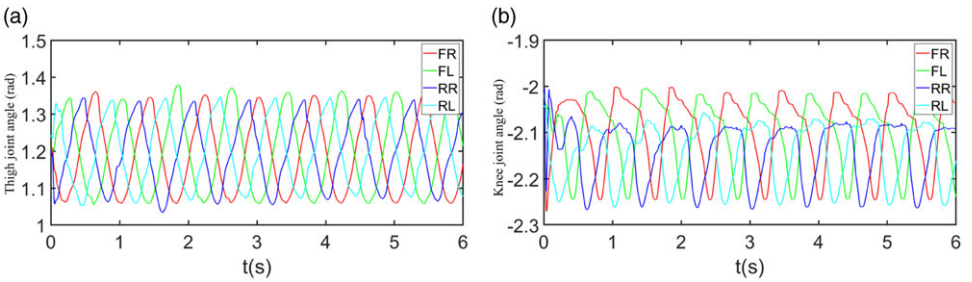


Figure 25. *Changes of leg joint angles during the execution of walking gait in the quadruped robot based on GD-CPG. (a) Thigh joint, (b) Knee joint.*

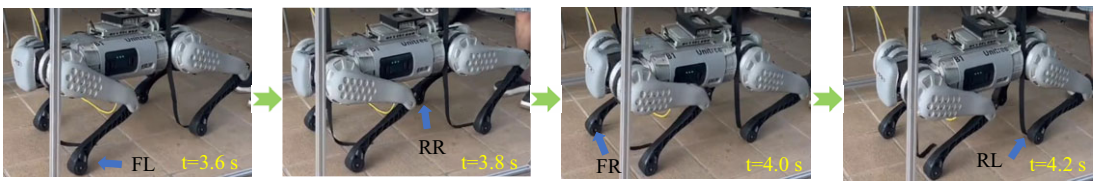


Figure 26. *Snapshots of GD-CPG-based quadruped robot executing walking gait.*

is biased toward the tail position at the midpoint of the body, and the center of gravity of the robot is leaning backward, which results in the knee joint of the rear leg being subjected to more pressure than that of the knee joint of the front leg in the support phase, and the knee joint of the rear leg rotates at a larger angle in the negative direction. The knee position curve fluctuates greatly in the support phase and does not show a flat state, which is caused by the friction force generated when the foot end of the corresponding leg contacts the ground is too large. In the experiment, each leg of the robot contacted the ground in sequence, and the phase sequence was FL–RR–FR–RL, which was a typical walking gait and conformed to the experimental expectation.

Figures 27 and 28 show the changes in the thigh and knee joint angles of each leg and the experimental snapshots of the quadruped robot during the execution of the trot gait, respectively. Due to the limitation of experimental conditions, the leg swing frequency was not set too large. From Figure 27a, it can be seen that the thigh joint angle varies from 1.07 rad to 1.34 rad during the quadruped robot's movement,

https://doi.org/10.1017/S0263574724001309 Published online by Cambridge University Press

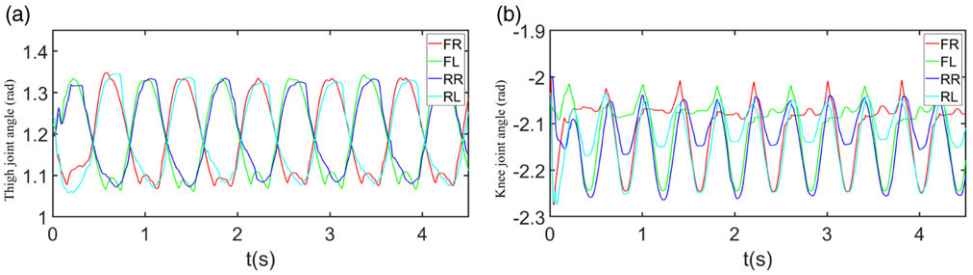


Figure 27. *Changes of leg joint angles during the execution of galloping gait in the quadruped robot based on GD-CPG. (a) Thigh joint, (b) knee joint.*

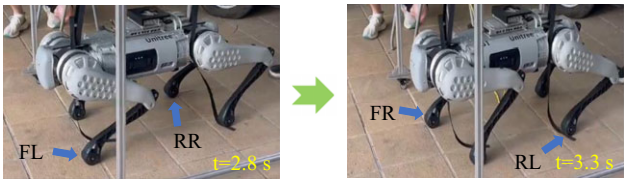


Figure 28. *Snapshots of GD-CPG-based quadruped robot executing galloping gait.*

and the knee joint (Figure 27b) exhibits a half-wave in the swing phase, with the maximum angle of rotation of about –2.25 rad; in the support phase, the knee joints slightly deviated from the equilibrium position, which was also caused by the body's center of gravity deviating backward. In addition, the knee joints of both rear legs show obvious flex in the support phase, with an angle of –2.15 rad. It is because under the condition that the quadruped robot does not move fast, the body supported by only two legs will tend to roll sideways to the left or right rear due to the shift of the center of gravity, resulting in excessive pressure on the knee joints of the rear legs. During the experimental time, the diagonal side legs of the robot constitute one group and the other group alternately contacting the ground movement, with the phase sequence of (FL, RR) – (FR, RL), which is a typical trotting gait and conforms to the experimental expectation.

The experimental results demonstrate that the GD-CPG-based quadruped robot can accomplish walking and trotting gait motions in real-world environments, verifying the feasibility of the GD-CPG control method.

6.2. Experiment based on the hexapod robot

The hexapod robot system in this experiment is mainly composed of a control board, servos, stand, power supply, and software. The leg servos are composed of 18 serial bus servos LX-224HV, whose technical specifications are shown in Table X.

In this experiment, a program is written based on GD-CPG and BI-GD-CPG fitting models to control the hexapod robot to perform tripod, tetrapod, and wave gait motions in a real environment. The parameter settings of GD-CPG are shown in Table XI.

Figure 29 shows the snapshots of the motion of the hexapod robot during the experiment. From Figure 29a, it can be seen that the two sets of legs of the hexapod robot move sequentially and alternately in a triangular contact with the ground, with a phase sequence of (FL, RL, MR) – (FR, RR, ML), which is a typical tripod gait. From Figure 29b, it can be seen that the hexapod robot's opposite side asymmetric three sets of legs contact the ground movement in sequence, the phase sequence is (FL, MR) – (ML,

https://doi.org/10.1017/S0263574724001309 Published online by Cambridge University Press

Table X. *Technical specifications of the serial bus servo LX-224HV.*

Parameters	**Values**
Size	$40 \times 20 \times 51$mm
Motor	DC iron core carbon brush motor
Connector type	PH2 3P
Operating voltage	11.1 V
Torque	20 kg.cm
Angle of rotation	0.0∼5.0 rad
Speed of rotation	0.18 sec/rad

Table XI. *GD-CPG parameter setting for the hexapod robot.*

Parameters	ω_i	ω_p	ω_q	R_i	C_i	a_i	φ_1	φ_2	φ_3	φ_4	φ_5	φ_6
Tripod gait	$\frac{\pi}{10}$	–	–	5.5	0	2.0	0	π	0	π	0	π
Tetrapod gait	–	$\frac{\pi}{10}$	$\frac{\pi}{20}$	5.5	0	2.0	0	$\frac{2\pi}{3}$	$\frac{4\pi}{3}$	$\frac{4\pi}{3}$	0	$\frac{2\pi}{3}$
Wave gait	–	$\frac{\pi}{10}$	$\frac{\pi}{50}$	5.5	0	2.0	0	$\frac{\pi}{3}$	$\frac{2\pi}{3}$	π	$\frac{4\pi}{3}$	$\frac{5\pi}{3}$

RR) - (RL, FR), which is a typical tetrapod gait. From Figure 29c, it can be seen that the hexapod robot six legs on both sides of the body move in wave-like contact with the ground in sequence, and the phase sequence is FL–ML–RL–FR–MR–RR, which is a typical wave gait.

The experimental results demonstrate that the GD-CPG-based hexapod robot can accomplish tripod, tetrapod, and wave gait motions in real-world environments, verifying the feasibility of the GD-CPG control method.

7. Conclusion

This article investigates the motion control problems of legged robots, including how to accomplish characteristic gait motions, improve the ability of legged robots to cope with complex terrains as well as enhance motion stability, linear motion capability, and motion speed. In this article, a motion control system is designed for the legged robot based on a lightweight CPG oscillator model, and simulation experiments are designed for verification. First, this article presents the first motion control method for legged robots based on GD-CPG. It is composed of a network of CPG oscillators and a legged robot motion mapping function, which provides higher execution efficiency compared to other common CPG models. Gait simulations verify the control method's validity, robustness, and transferability. To improve the ability of the legged robot to cope with complex terrain, this article proposes a motion control method for the legged robot based on RG-CPG. Compared with the traditional vestibular sensory feedback model that only balances the body pitch, this article also adds the balancing functions of body roll and yaw, which can balance the quadruped robot's body attitude from more dimensions and improve the linear motion ability. Simulation verifies the validity of the control method. Then, this article introduces the DE algorithm and designs the motion fitness function in RG-CPG to achieve adaptive optimization of vestibular sensory feedback parameters. In addition, this article highlights the superiority of the RG-CPG control method by comparing it with two other existing CPG control methods. Finally, this article concludes with physical experiments, which verify the feasibility of the control method in the real world.

However, there are some shortcomings in the work of this article. First, the biological vestibular sensory feedback mechanism is only established in the control system of a quadruped robot. For other types of legged robots, the feedback mechanism for balancing the body motion attitude is not established according to their structural and gait characteristics. The RG-CPG transportability cannot be verified. Second, for the design of the motion adaptability function of legged robots, this article only considers

https://doi.org/10.1017/S0263574724001309 Published online by Cambridge University Press

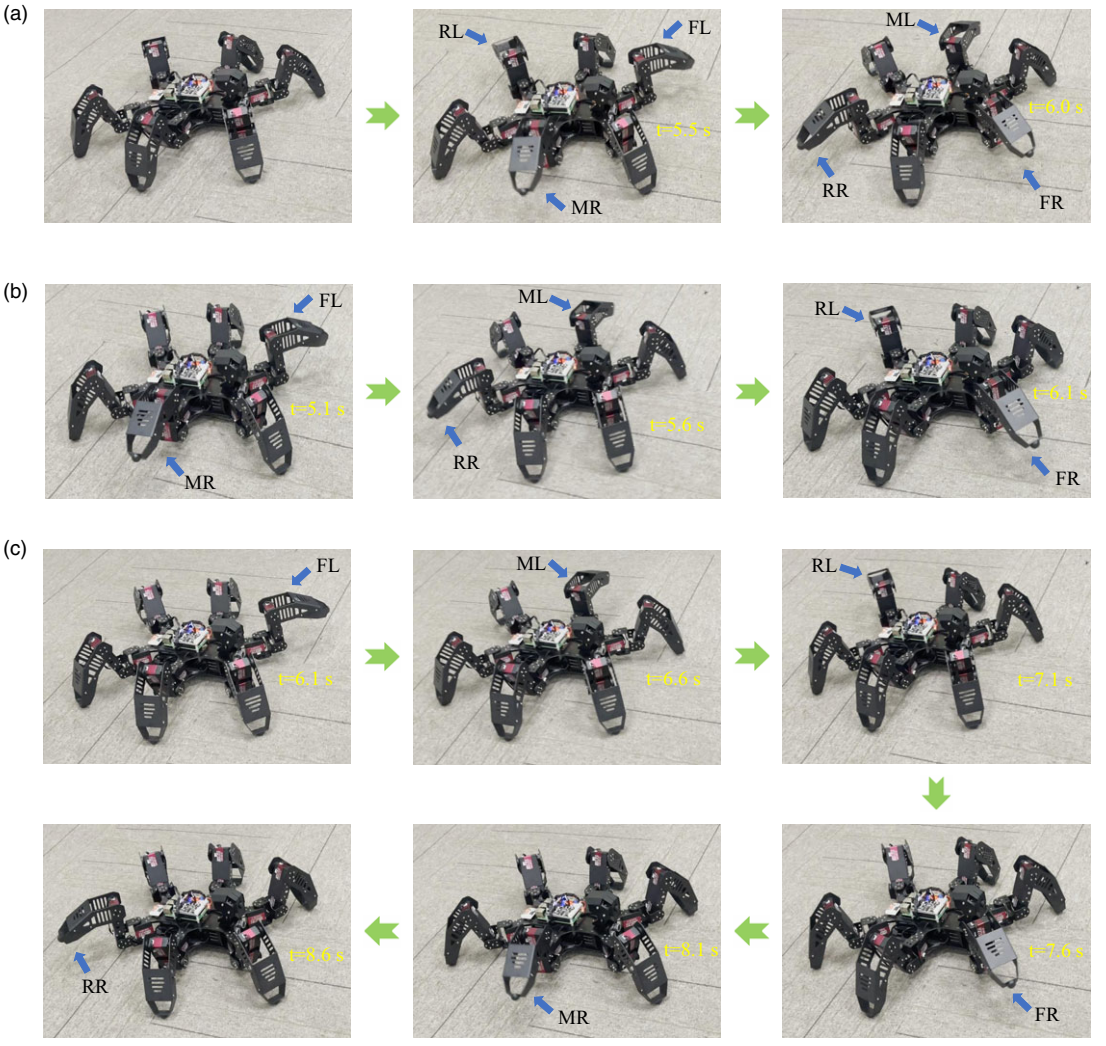


Figure 29. *Snapshots of hexapod robot executing three gaits based on GD-CPG and BI-GD-CPG fitting. (a) Tripod gait, (b) Tetrapod gait, (c) Wave gait.*

the two factors of motion stability and motion speed and does not take into account the motion accuracy, flexibility, and energy consumption during the motion process.

Author contributions. N. Tan conceived and designed the research and provided relevant resources. Y. Zhang designed the algorithms, implemented the system, and drafted the paper. Y. Zhang and W. Liu conducted data gathering and performed statistical analyses. Y. Zhang and N. Tan wrote and revised the manuscript.

Financial support. This research was supported by the National Natural Science Foundation of China (62173352) and the Guangdong Basic and Applied Basic Research Foundation (2024B1515020104).

Competing interests. The authors declare no conflicts of interest exist.

Ethical Standard. Not applicable.

Data availability. Video files are available from the authors upon request.

https://doi.org/10.1017/S0263574724001309 Published online by Cambridge University Press

References

[1] J. Chen, Y. Liu, J. Zhao, H. Zhang and H. Jin, "Biomimetic design and optimal swing of a hexapod robot leg," *J. Bionic. Eng.* **11**(1), 26–35 (2014).

[2] Y. Zhao, X. Chai, F. Gao and C. Qi, "Obstacle avoidance and motion planning scheme for a hexapod robot octopus-iii," *Robot. Auton. Syst.* **103**, 199–212 (2018).

[3] A. J. Ijspeert, "Central Pattern Generators for Locomotion Control in Animals and Robots: A Review," **In:** *Neural Networks*, vol. **21** (Robotics and Neuroscience, 2008) pp. 642–653.

[4] J. Ostrowski and J. Burdick, "Geometric Perspectives On the Mechanics and Control of Robotic Locomotion," **In:** *Robotics Research* (G. Giralt and G. Hirzinger, eds.) (Springer London, London, 1996) pp. 536–547.

[5] N. Hogan and D. Sternad, "On rhythmic and discrete movements: Reflections, definitions and implications for motor control," *Exp. Brain. Res.* **181**(1), 13–30 (2007).

[6] F. Delcomyn, "Neural basis of rhythmic behavior in animals," *Science* **210**(4469), 492–498 (1980).

[7] S. Grillner, "Neurobiological bases of rhythmic motor acts in vertebrates," *Science* **228**(4696), 143–149 (1985).

[8] S. L. Hooper, "Central pattern generators," *Curr. Biol.* **10**(5), R176–R179 (2000).

[9] M. A. Lewis and L. S. Simo, "A Model of Visually Triggered Gait Adaptation," *Proc. of AMAM* **21**(3), 2350016 (2024).

[10] J. Yu, M. Tan, J. Chen and J. Zhang, "A survey on CPG-inspired control models and system implementation," *IEEE Trans. Neur. Net. Lear. Syst.* **25**(3), 441–456 (2014).

[11] H. Zheng, X. Zhang, T. Li and G. Duan, "Robot motion control method based on CPG principle," *Chinese High Technol. Lett.* **13**(7), 64–68 (2003).

[12] C. Liu, D. Wang and Q. Chen, "Central pattern generator inspired control for adaptive walking of biped robots," *IEEE Trans. Syst. Man Cybern.: Syst.* **43b**(5), 1206–1215 (2013).

[13] M. Wang, Y. Zhang and J. Yu, "An SNN-CPG hybrid locomotion control for biomimetic robotic fish," *J. Intell. Robot. Syst.* **105**(2), 1–25 (2022).

[14] J. Yu, Z. Wu, X. Yang, Y. Yang and P. Zhang, "Underwater target tracking control of an untethered robotic fish with a camera stabilizer," *IEEE Trans. Syst. Man Cybern.: Syst.* **51**(10), 6523–6534 (2021).

[15] H. Yu, H. Gao, L. Ding, M. Li, Z. Deng and G. Liu, "Gait generation with smooth transition using CPG-based locomotion control for hexapod walking robot," *IEEE Trans. Ind. Electron.* **63a**(9), 5488–5500 (2016).

[16] C.-S. Park, Y.-D. Hong and J.-H. Kim, "Evolutionary-optimized central pattern generator for stable modifiable bipedal walking," *IEEE/ASME Trans. Mechatron.* **19**(4), 1374–1383 (2014).

[17] G. Zhong, L. Chen, Z. Jiao, J. Li and H. Deng, "Locomotion control and gait planning of a novel hexapod robot using biomimetic neurons," *IEEE Trans. Contr. Syst. Technol.* **26**(2), 624–636 (2018).

[18] S. Du, Z. Wu, J. Wang, S. Qi and J. Yu, "Design and control of a two-motor-actuated tuna-inspired robot system," *IEEE Trans. Syst. Man Cybern.: Syst.* **51**(8), 4670–4680 (2021).

[19] Z. Wang, Q. Gao and H. Zhao, "CPG-inspired locomotion control for a snake robot basing on nonlinear oscillators," *J. Intell. Robot. Syst.* **85**(2), 209–227 (2017).

[20] Y. Mao and Z. Zhang, "Asymptotic frequency synchronization of kuramoto model by step force," *IEEE Trans. Syst. Man Cybern.: Syst.* **50**(8), 2768–2778 (2020).

[21] J. Pan, Z. Zhou, J. Wang, P. Zhang and J. Yu, "Development of a penguin-inspired swimming robot with air lubrication system," *IEEE Trans. Ind. Electron.* **70**(3), 2780–2789 (2023).

[22] J. Jo, G. Park and Y. Oh, "Robust walking stabilization strategy of humanoid robots on uneven terrain via QP-based impedance/admittance control," *Robot. Auton. Syst.* **154**, 104148 (2022).

[23] YAT. S., "Robust walking and running gaits for biped robots with a QP-based whole-body controller," *Int. J. Hum. Robot.* **2350016**, 18 (2023).

[24] R. Fazel, A. Shafei and S. Nekoo, "Dynamic modeling and closed-loop control design for humanoid robotic systems: Gibbs–appell formulation and sdre approach," *Multibody. Syst. Dyn.* **62**(1), 57–86 (2024).

[25] H. Zheng, X. Zhang, Z. Cheng, L. Zhao, X. Guan, P. Liu and X. Tang, *Biologically-Inspired Motion Control Theory and Its Application for a Legged-Robot* (Tsinghua University Press, Beijing, 2011).

[26] X. Zhang, Q. Wang, S. Huang and L. Jiang, "A multi-model fusion based complex motion control approach for a cheetah-mimicking quadruped robot," *Robot* **44**(6), 682–693 (2022).

[27] L. Xu, W. Liu, Z. Wang and W. Xu, "Gait Planning Method of a Hexapod Robot Based on the Central Pattern Generators: Simulation and Experiment," *In IEEE International Conference on Robotics and Biomimetics*, IEEE (2013) pp. 698–703.

[28] C. Bal, "Neural coupled central pattern generator based smooth gait transition of a biomimetic hexapod robot," *Neurocomputing* **420**, 210–226 (2021).

[29] J. H. Barron-Zambrano, C. Torres-Huitzil and B. Girau, "Perception-driven adaptive CPG-based locomotion for hexapod robots," *Neurocomputing* **170**, 63–78 (2015).

[30] G. Sartoretti, S. Shaw, K. Lam, N. Fan, M. Travers and H. Choset, "Central Pattern Generator with Inertial Feedback for Stable Locomotion and Climbing in Unstructured Terrain," *IEEE International Conference on Robotics and Automation*, IEEE (Springer Nature, 2018) pp. 5769–5775.

[31] R. Pérez-López, A. Espinal, M. Sotelo-Figueroa, E. I. Guerra-Hernandez, P. Batres-Mendoza and H. Rostro-Gonzalez, *Evolutionary Deployment of Central Pattern Generators for Legged Robots Using Nengo* (Springer Nature Switzerland, Cham, 2024) pp. 141–155.

[32] G. Chen, Y. Xu, X. Yang, H. Hu, H. Cheng, L. Zhu, J. Zhang, J. Shi and X. Chai, "Target tracking control of a bionic mantis shrimp robot with closed-loop central pattern generators," *Ocean. Eng.* **297b**, 116963 (2024).

https://doi.org/10.1017/S0263574724001309 Published online by Cambridge University Press

[33] Y. Wu, S. Guo, Z. Yu, P. Wang, L. Niu and M. Song, "Design of an optimized gait planning generator for a quadruped robot using the decision tree and random forest workspace model," *Robotica* **41**(12), 3746–3771 (2023).
[34] G. Chen, Y. Han, Y. Li, J. Shen, J. Tu, Z. Yu, J. Zhang, H. Cheng, L. Zhu and F. Dong, "Autonomous gait switching method and experiments of a hexapod walking robot for mars environment with multiple terrains," *Intel. Serv. Robot.* **17**(3), 533 (2024).
[35] T. Fukui, H. Fujisawa, K. Otaka and Y. Fukuoka, "Autonomous gait transition and galloping over unperceived obstacles of a quadruped robot with CPG modulated by vestibular feedback," *Robot. Auton. Syst.* **111**, 1–19 (2019).
[36] T. Fukui, S. Matsukawa, Y. Habu and Y. Fukuoka, "Gait transition from pacing by a quadrupedal simulated model and robot with phase modulation by vestibular feedback," *Robotics* **11**(1), 6523–6534 (2022).
[37] Y. Fukuoka, Y. Habu and T. Fukui, "Analysis of the gait generation principle by a simulated quadruped model with a CPG incorporating vestibular modulation," *Biol. Cybern.* **107**(6), 695–710 (2013).
[38] C. Liu, Q. Chen and G. Wang, "Adaptive walking control of quadruped robots based on central pattern generator (CPG) and reflex," *J. Control Theory Appl.* **11a**(3), 386–392 (2013).
[39] S. Gay, J. Santos-Victor and A. Ijspeert, "Learning Robot Gait Stability using Neural Networks as Sensory Feedback Function for Central Pattern Generators," *2013 IEEE/RSJ International Conference on Intelligent Robots and Systems*, IEEE (2013) pp. 194–201.
[40] T. Srinivas, A. K. K. Madhusudhan, L. Manohar, N. M. S. Pushpagiri, K. C. Ramanathan, M. Janardhanan and I. Nielsen, "Valkyrie–design and development of gaits for quadruped robot using particle swarm optimization," *Appl. Sci.* **11**(16), 7458 (2021).
[41] M. Wang, H. Dong, X. Li, Y. Zhang and J. Yu, "Control and optimization of a bionic robotic fish through a combination of CPG model and PSO," *Neurocomputing* **337a**, 144–152 (2019).
[42] S. Wang, Q. Shi, J. Gao, Y. Wang, F. Meng, C. Li, Q. Huang and T. Fukuda, "Design and Control of a Miniature Quadruped Rat-Inspired Robot," *2019 IEEE/ASME International Conference on Advanced Intelligent Mechatronics (AIM)*, Tokyo, Japan, IEEE (2019) pp. 346–351.
[43] J. Yu, Z. Wu, M. Wang and M. Tan, "CPG network optimization for a biomimetic robotic fish via PSO," *IEEE Trans. Neur. Net. Lear. Syst.* **27b**(9), 1962–1968 (2016).
[44] Y. Hu, J. Liang and T. Wang, "Parameter synthesis of coupled nonlinear oscillators for CPG-based robotic locomotion," *IEEE Trans. Ind. Electron.* **61**(11), 6183–6191 (2014).
[45] Y. Farzaneh, A. Akbarzadeh and A. A. Akbari, "New automated learning CPG for rhythmic patterns," *Intel. Serv. Robot.* **5**(3), 169–177 (2012).
[46] Z. Bing, L. Cheng, G. Chen, F. Röhrbein, K. Huang and A. Knoll, "Towards autonomous locomotion: CPG-based control of smooth 3D slithering gait transition of a snake-like robot," *Bioinspir. Biomim.* **12a**(3), 035001 (2017).
[47] Z. Bing, L. Cheng, K. Huang, M. Zhou and A. Knoll, "CPG-Based Control of Smooth Transition for Body Shape and Locomotion Speed of a Snake-like Robot," In *2017 IEEE International Conference on Robotics and Automation (ICRA)*, IEEE (Springer Nature, 2017) pp. 4146–4153.
[48] B. A. Pearlmutter, "Gradient calculations for dynamic recurrent neural networks: a survey," *IEEE Trans. Neur. Net.* **6**(5), 1212–1228 (1995).
[49] P. Li, Research On Gait of Hexapod Robot Based On Cpg and Reinforcement Learning *Master's thesis* (Hangzhou Dianzi University, 2022).
[50] C. Bai, Optimal Design of the Parallel Leg Mechanism and CPG Based Locomotion Control for a Quadruped Robot *Master's thesis* (Harbin Institute of Technology, 2021).
[51] R. Storn and K. Price, "Differential evolution–a simple and efficient heuristic for global optimization over continuous spaces," *J. Glob. Optim.* **11**(4), 341–359 (1997).
[52] J. Liu, *Intelligent Control* (IEEE, 2021).

Cite this article: Y. Zhang, W. Liu and N. Tan (2024). "Motion control of legged robots based on gradient central pattern generators", Robotica **42**, 3102–3131. https://doi.org/10.1017/S0263574724001309

https://doi.org/10.1017/S0263574724001309 Published online by Cambridge University Press